The impact of storms, wind and vegetation recovery on washover development on Rottumeroog, studied using high-resolution satellite imagery

MSc thesis

Yaron Huberts

Student number: 5520193

Universiteit Utrecht

Department of Physical Geography

Supervisors: dr. M. van der Vegt & prof. dr. B.G. Ruessink

March 2020

2nd version

Preface

This study was performed as part of my MSc thesis, which I carried out from June 2019 to January 2020. I would like to thank everyone who helped and supported me in writing this thesis, in particular my family, my supervisors, dr. M. van der Vegt and prof. dr. B.G. Ruessink, and my friends and fellow students at Utrecht University, most notably Loek Schemmekes and Bart Maas, who also used Planet satellite imagery for their theses. We cooperated intensively, especially regarding the pre-processing and the image analysis in Matlab, and I believe that our mutual cooperation aided the development of our own theses. I would also like to thank Planet Labs, Inc. for providing the satellite imagery needed for this study and to provide the data free of charge for educational purposes, as I would never have been able to perform this thesis otherwise.

Table of contents:

Abstract

Washover openings are naturally occurring, low-lying features on barrier islands, which occasionally experience overwash. Allowing washovers on barrier islands is currently being considered in order to increase the sediment supply and to allow the islands to accrete with sea-level rise. However, washover evolution has not been researched extensively, and studies so far have used a coarse temporal resolution. This study has investigated the evolution of a washover on Rottumeroog from 2009 to 2019, on both a long-term and on a seasonal timescale, using high-resolution satellite imagery with a spatial resolution of 3 to 5 metres and weekly to monthly coverage. The satellite imagery was classified using a pixel-based classification and compared to supporting data. It was found that the washover formed in 2012. At first, the washover was sheltered by dunes to the northeast, which likely reduced the frequency of overwash events. When these dunes were eroded in 2014, the washover rapidly expanded to the south and west, until it reached higher areas beyond which the washover could not expand. The expansion of the washover was coupled with a southward migration of the island as the beach was eroded as sediment from the beach was deposited in the washover. The washover showed strong seasonal patterns in vegetation growth as a result of washover frequency: All inundation events occurred from October to April. After the overwash season in winter and early spring, vegetation starts to grow in the washover as conditions become more favourable, demonstrating that vegetation can already develop in a washover shortly after overwash. As washovers start to occur in late autumn, vegetated areas change to sandy areas and conditions become unfavourable for vegetation growth. When the washover was sheltered by the dunes, conditions were more favourable for vegetation than after these dunes were eroded in 2014. Vegetation regrowth was high again (~70% ±10% of the washover area) from 2016 onwards, which is likely because of an increase in elevation as a result of overwash. Aeolian changes were common in spring but not in other months, as vegetation reduces the fetch in summer and the sand is too wet in winter because of the frequent overwash. Overwash was dominant in determining the long-term evolution of the washover, while aeolian transport did not lead to any permanent changes in land cover.

1. Introduction

Washover openings are naturally occurring, low-lying features on barrier islands, which occasionally experience overwash. Figure 1.1 shows two examples of washovers on barrier islands in the Wadden Sea.

Washover formation results in the destruction of the foredune, eroding a large volume of sand, which is generally deposited onshore (Hosier & Cleary, 1977; Aagaard & Kroon, 2019). The initial erosion of the foredune makes the area more susceptible to future washovers (Mathew et al., 2010), and they are often reactivated and enlarged by following storms (Sedrati et al., 2010; Aagaard & Kroon, 2019). High accretion rates during overwash result in washovers being very effective in causing a net increase in elevation (Nielsen & Nielsen, 2006; Aagaard & Kroon, 2019).

Washover openings have mostly disappeared from the Dutch Wadden Islands as the islands were closed off by sand drift dikes (Oost et al., 2012). Re-activation of washover complexes in uninhabited areas is currently being considered by the Dutch coastal zone management (Wesselman et al., 2017; Wesselman, 2019). This would lead to additional sand deposition on the barrier islands, allowing them to grow with sea-level rise in a natural way. This would also allow for more biodiversity as pioneer species colonise areas previously occupied by the climax vegetation (Hoekstra et al., 2009, Oost et al., 2012).

Washover formation has been studied extensively, but washover evolution after washover formation has received little attention in the past (Aagaard & Kroon, 2019), and the studies which have been done have often focused on hurricane-driven, low-lying systems (e.g. Durán Vinent & Moore, 2014), which differ significantly from barrier islands in the Wadden Sea. Past studies include Mathew et al. (2010) who studied the evolution of a washover in Canada since 1936 using aerial photographs, and Nielsen & Nielsen (2006) and Aagaard & Kroon (2019) who investigated the development of washover in Denmark since 1990 using grounds surveys. Aagaard & Kroon also included two LiDAR datasets to support their findings. These studies show that washover evolution on a multi-year scale is marked by re-activation of the washover on one hand, which leads to increased accretion, and by the recovery of the dune system and aeolian transport on the other hand, which eventually leads to the washover disappearing.

Washover evolution on a seasonal scale has not been the subject of any specific studies and is poorly understood, though some observations have been made (e.g. Sedrati et al., 2010; Aagaard & Kroon, 2019). Overwash events can follow strong seasonal patterns (Sedrati et al., 2010), but seasonal patterns in washover evolution have not been observed so far.

This study aims to increase the understanding of washover evolution on both a seasonal and a multi-year time scale. This will be achieved by the study of the evolution of a natural washover on Rottumeroog from 2009 to 2019, using high-resolution remote sensing data. Past studies examining washover evolution had a temporal resolution ranging from once to year (for surveys; Aagaard & Kroon, 2019) to once a decade (Mathew et al., 2010). In contrast, this study will use a temporal resolution of typically several images a month, or even multiple images a week, which will allow for a more in-depth investigation of washover evolution on several

timescales. This study will increase our understanding of the evolution of washovers and on the impacts which these systems can have.

The main research question of this study is:

What are the effects of storms, wind and vegetation recovery on washover evolution on Rottumeroog?

This study will first present a summary of the existing literature (Chapter 2.1) and a description of the study area (Chapter 2.2), which will be used to formulate the hypotheses (Chapter 2.3). Afterwards, the methods will be discussed (Chapter 3), and the results will be presented (Chapter 4) and evaluated (Chapter 5). Finally, the conclusions will be given (Chapter 6).

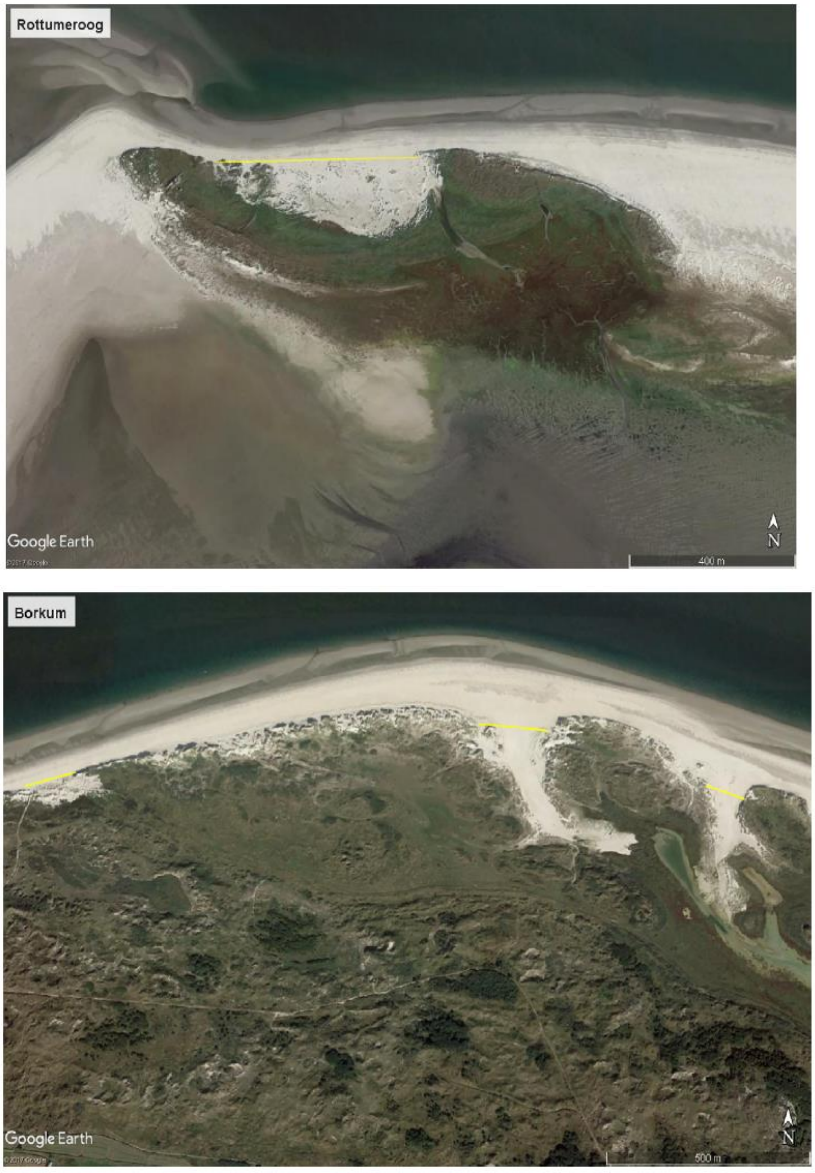

Figure 1.1. Source: Wesselman et al., 2019.
Top: Satellite image of a washover on Rottumeroog. Bottom: Satellite image of a washover on Borkum.

2. Theoretical framework

2.1. Literature review

This chapter will first discuss the occurrence of washovers and the evolution of barrier islands. Afterwards, the mechanisms governing their evolution. Afterwards, the observed long-term trends in washover evolution will be considered. Finally, washover evolution on a seasonal scale will be discussed.

2.1.1. Barrier islands

Figure 2.1 shows a conceptual map of a barrier island in the Wadden Sea. Barrier islands typically contain large dune arcs in the west. Washover complexes are typically found at the end of the dune arc, and on the island tail, where dunes alternate with washover fans (Oost et al., 2012). Salt marshes typically occur on the lagoon (Wadden Sea) side of the island.

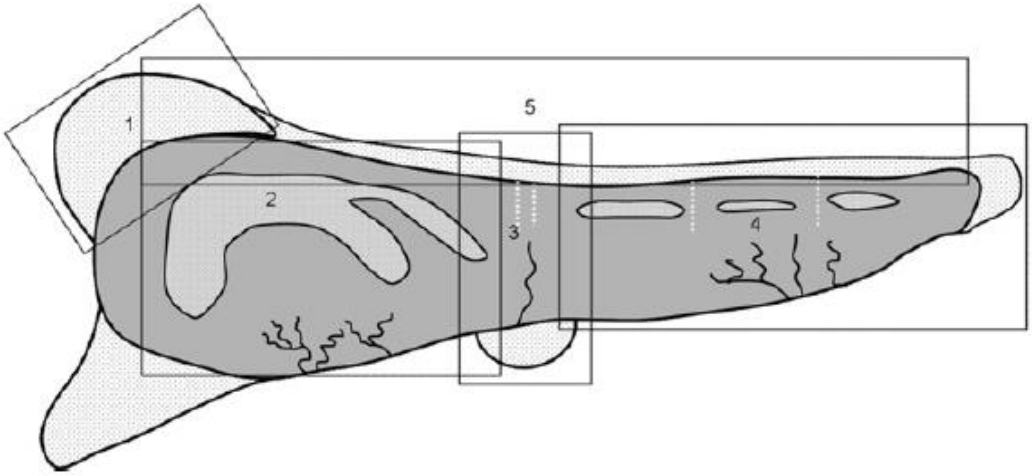

Figure 2.1. Source: Oost et al., 2012, after Löffler et al., 2008. Conceptual map of a barrier island showing the five main morpho-ecological units: (1) island head; (2) dune arc; (3) washover complex; (4) island tail (5) beach and shoreface. Smaller washovers are also found between the dunes at (4), denoted by the dotted white lines.

Barrier island evolution is controlled by storm erosion and sea-level rise on one hand, and aeolian and biological processes, which drive dune recovery, on the other hand. Barrier islands tend to be bistable: when dune recovery dominates, islands are high in elevation with low storm vulnerability, while when storm erosion dominates, islands are low and storm vulnerability is maximised. Higher islands typically have well-developed dunes which resist storms, while lower islands often lack vegetated dunes. When sea-level rise dominates, barrier islands become unstable and drown (Durán Vinent & Moore, 2014), or migrate landward if overwash sediment fluxes are insufficient to keep up with sea-level rise (Lorenzo-Trueba & Ashton, 2013). If the barrier width falls below a critical threshold, overwash becomes increasingly frequent and the island can enter a rollover phase (Lorenzo-Trueba & Ashton, 2013).

2.1.2. Sediment transport dynamics

At the Wadden Islands, sediment transport in washovers is dominated by cross-shore currents, which are generated by a combination of tidal water levels, storm surges and wave set-up (Wesselman et al., 2019). Wesselman et al. (2019) found that waves mainly dissipate at a subtidal sandbar and at the foreshore. At the Wadden Islands, short and infragravity waves typically dominate the sand transport from the shoaling zone until the washover crest, after which the mean flow becomes more important (Engelstad, 2019).

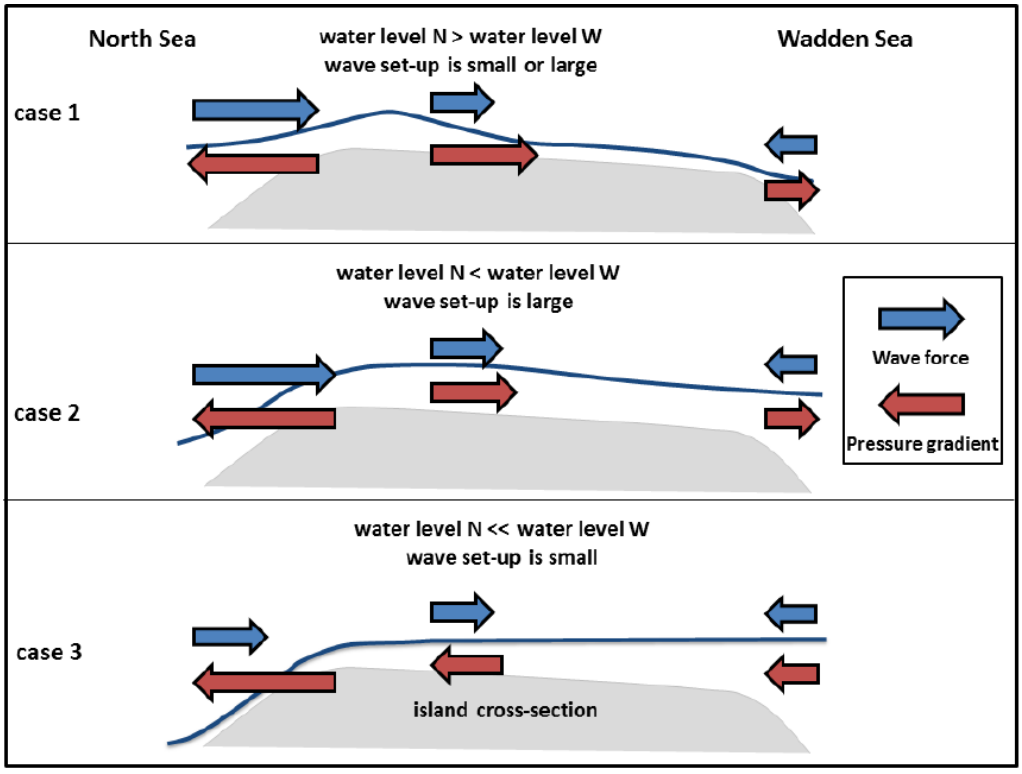

Figure 2.2. Source: Engelstad, 2017.
Conceptual cross-section of a barrier island, showing the two main forces driving the flow during inundation, the wave force and the pressure gradient, for various cases. Water levels are shown in blue.

Wave breaking leads to wave set-up in the washover during inundation. This set-up decreases from the washover in the landward direction as most wave energy has already been dissipated. This drives a cross-shore current from the washover opening in the onshore direction as a pressure gradient is generated (see Figure 2.2). At the Wadden Islands, a pressure gradient was usually generated from the North Sea towards the Wadden Sea, resulting in an onshore flow in the washover during rising tide (Wesselman et al., 2019), with peak velocities shortly before maximum tide (Engelstad, 2019; see Figure 2.2, case 1). At the Wadden Islands, high tide water levels are typically higher in the Wadden Sea than in the North Sea. During falling tide, a pressure gradient is generated from the Wadden Sea towards the North Sea (see Figure 2.2, case 2). This partially counteracts the onshore sediment transport induced by the waves. This results in a low onshore sediment flux or an offshore sediment flux during low tide. However, total

sediment over a tidal cycle transport flux is onshore (Hoekstra et al., 2009, Engelstad, 2019, Wesselman et al., 2019), and sediment transport is only rarely seaward. Even with higher water levels in the Wadden Sea than in the North Sea, the mean flow can still be onshore; the exact mechanisms depend on the inundation event, as the higher tidal water levels in the Wadden Sea are often compensated by the wave set-up in the North Sea (Engelstad, 2019).

About 50 metres offshore of the washover opening, the beach shows an eroding trend as the flow accelerates because of flow convergence. As flow convergence increases into the washover, the erosion also increases. On the landward side of the washover, sediment is deposited as currents decelerate because of flow expansion (Wesselman et al., 2019).

2.1.3. Long-term washover evolution

Washover formation results in the destruction of the foredune, eroding a large volume of sand (Hosier & Cleary, 1977, Aagaard & Kroon, 2019). Part of this sand (in a washover in Denmark, it amounted to 36% of the eroded volume) is deposited inland, covering the old vegetation (such as salt marsh) and forming a washover fan (Aagaard & Kroon, 2019). The initial erosion of the foredune makes the area more susceptible to future overwash events (Mathew et al., 2010). Though washovers sometimes form in a single storm, they are often reactivated and enlarged by following storms (Sedrati et al., 2010; Aagaard & Kroon, 2019). Continued overwash can lead to the formation of a washover terrace, with little variation in elevation (Hosier & Cleary, 1977). There is considerable temporal variation in the storm surge frequency and duration (Aagaard & Kroon, 2019).

Re-activation of the washover occurs when the washover is inundated again. This causes the environment to become more saline, making it more difficult to colonise (Nielsen & Nielsen, 2006). Accretion rates can be very high during inundation (Nielsen & Nielsen, 2006; Aagaard & Kroon, 2019), and can result in the washover covering new areas (Sedrati et al., 2010). On a washover in Denmark, accretion rates were highest in period with high overwash frequencies and lowest in periods with low overwash frequencies. A single storm surge added more than 0.5 metres of sediment to the washover (Nielsen & Nielsen, 2006). These high accretion rates result in washovers being very effective in causing a net increase in elevation, despite the initial washover event eroding a large volume of sediment. An example of this can be seen in Figure 2.2, where the washover gains almost a metre in elevation between 1990 and 2000 as a result of overwash events. The continued high accretion (typically tens of $m^3/m/yr$; Mathew et al., 2010, Aagaard & Kroon, 2019, Wesselman, 2019) rates on washovers eventually make future overwash less likely, resulting in a lower overwash duration (Aagaard & Kroon, 2019). An exception is when the shoreface response rate is low: in this situation, the barrier geometry cannot be maintained, resulting in a decrease in island width and the disintegration of the island (Lorenzo-Trueba & Ashton, 2013).

The increased elevation makes it easier for vegetation to colonise the washover because of a decrease in salt stress (Aagaard & Kroon, 2019). Once the elevation of the washover exceeds a critical value, rainfall will be able to reduce the salinity of the washover, allowing for vegetation to colonise, and for increased aeolian sediment transport as the washover becomes well-drained

(Nielsen & Nielsen, 2006). This will lead to a recovery of the dune system (Durán Vinent & Moore, 2014). An alternative explanation was given for a washover in Canada, where pioneer vegetation took a long time to establish itself. This was hypothesised to imply that the large washover event removed the sources of the pioneer vegetation in the vicinity of the washover (Mathew et al., 2010).

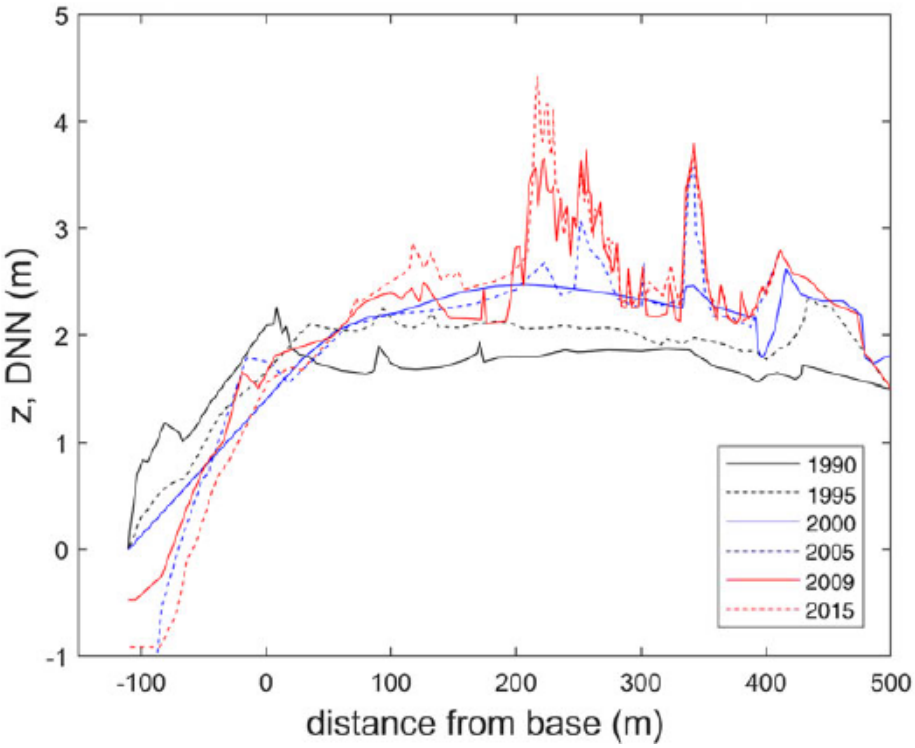

Figure 2.2. Source: Aagaard & Kroon, 2019.
Cross-shore profile along the central axis of a washover in Skallingen, Denmark.

It can take a significant time before the dune system starts to recover. For the washover in Figure 2.2, dunes only developed in 2005, 15 years after the washover was formed. In contrast, dunes at the sheltered landward part of the washover started to recover soon after the washover was formed. On a washover in Canada, it took more than 40 years for a continuous, vegetated foredune to develop (Mathew et al., 2010), as is shown in Figure 2.4. Figure 2.4 initially shows an increase in the area of both the foredunes and the fixed and mobile inland sand dunes. The mobile inland sand dunes eventually decrease in area while the foredunes and fixed inland sand dunes continue to increase as the dunes get vegetated.

As the washover is unvegetated, sand is easily brought into saltation. This implies that the prevailing wind direction is very important for the evolution of the washover. Aeolian dynamics on washovers have received little interest and only a few observations have been made. The relation between wind speed and duration and the sediment supply to the washover was found to be poor (Aagaard & Kroon, 2019). The reason for this is not known. It might be because of the strong influence of the wind direction or because the system is sediment-limited. On the

washover in Denmark, aeolian transport in a period with low overwash frequencies resulted in a lowering of the central part of the washover and an increase in elevation at the sides of the washover (Nielsen & Nielsen, 2006). Marginal vegetation was able to effectively trap saltating sediment. This is a form of positive feedback, as this aids the establishment of dune grasses, which are more efficient at trapping sediment. The recovery of the dunes in the central part of the washover coincided with a period of low overwash frequencies (Aagaard & Kroon, 2019).

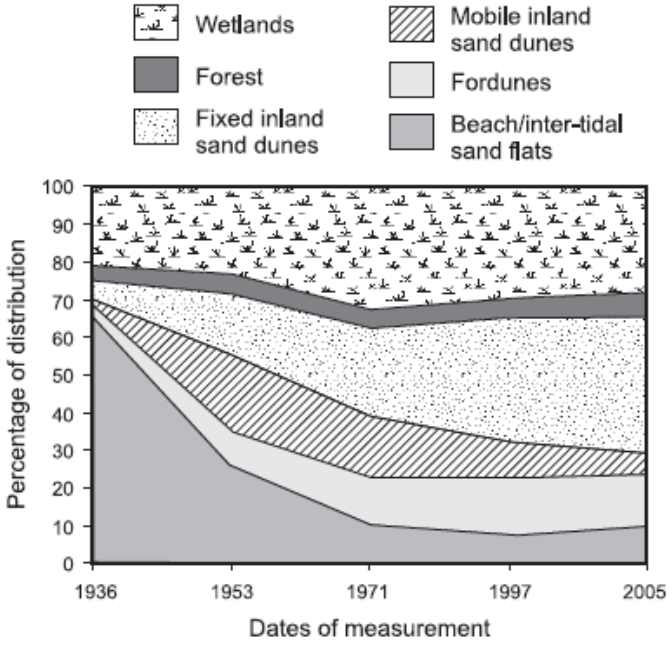

Figure 2.4. Source: Mathew et al., 2010.
Evolution of the area (in %) covered by different geomorphological units for a washover in Canada.

The evolution of the washover is often accompanied by a retreat of the beach as sediment is transported from the beach to the washover (Aagaard & Kroon, 2019, Nielsen & Nielsen, 2006, Wesselman, 2019). At Skallingen, the washover accretion greatly exceeded the erosion of the beach. Extra sediment was supplied to the beach by bar migration and welding (Aagaard & Kroon, 2019). However, this pattern of beach erosion is not universal: the coastline near a washover in Canada remained relatively stable for almost 70 years (Mathew et al., 2010). The sediment sources of this washover system were not studied in detail. It is thus not known if there was another sediment source was able to deliver sediment to the beach and/or the washover.

2.1.4. Washover evolution on a seasonal scale

Washover evolution on a seasonal scale has not been the subject of any specific studies, but some observations have been made, though most focused on the dynamics as opposed to the actual evolution of the washover. In general, washover evolution on a seasonal scale is not well understood. Seasonal patterns in washover evolution and dynamics will differ between regions with different climates. On Rottumeroog, they are likely most comparable with other washovers in north-eastern Europe. On a washover in Skallingen, Denmark, all overwash events occurred in the winter, from December till February (Aagaard & Kroon, 2019). Washovers on a barrier island

in Italy were predominantly in the winter as well, though this apparently did not lead to seasonal patterns in morphological development on an unvegetated washover (Sedrati et al., 2010). The reason for this is unknown. In Denmark, aeolian saltation was found to be most common in the autumn and winter months. The NAO-index (North Atlantic Oscillation) was also found to be an indicator for the sediment supplied to the washover. A positive NAO-index indicates below-normal pressures in the North Atlantic, which is associated with intense westerly winds and larger than average waves at the Danish North Sea coast. During the winter, the NAO-index scaled with sediment supply, while there was no relationship in summer. The likely reason for this is that the NAO gives an indication of both the wind speed and duration and the wave climate, both of which influence washover processes (Aagaard & Kroon, 2019).

2.2. Study area

Rottumeroog is an uninhabited Wadden island between the North Sea and the Wadden Sea (see Figure 2.5). It is about 0.5-1 kilometres wide and approximately 3 kilometres long (Wesselman, 2019). Rottumeroog is the easternmost Dutch Wadden island, and it is situated between two tidal channels on eastern and the western side of the island. The Ems-Dollard estuary is about two kilometres to the east of the tidal channel on the eastern side of Rottumeroog. Since 1990, the Dutch coastline has been kept in place with nourishments. However, Rottumeroog has been excluded from this policy since 2005, allowing the island to evolve naturally (Wesselman, 2019). There is a large amount of spatial and temporal variation in elevation, but the highest dunes are typically up to 8 metres high, while the vast majority of the island has a much lower elevation. The dunes are concentrated on the northern (North Sea) side of the western and central part of the island, and on the southwestern side of the island. The area behind the dunes, on the Wadden Sea side, consists largely of a low-lying salt marsh. The eastern part of the island forms a low-lying island tail.

Figure 2.5. Source: Wesselman, 2019. Location of Rottumeroog. Image from Google Earth, 21-05-2018.

This study expands on previous work by Wesselman (2019), who investigated the long-term evolution of the washover on Rottumeroog between 2005 and 2017 using DEMs. This

section will give a summary of his work and provide an overview of the geography and evolution of the island.

On the first DEMs, from 2005 and 2007, the washover system is not yet visible (Figure 2.6a & b; Wesselman, 2019). There are two major dune rows visible: one running from the westernmost point of the island along the southern coast, where it gradually decreases in elevation. The other dune row is on the northern side of the island and is bordered by relatively lower areas to the east and west, of about 2 to 4 metres in elevation. As the island is bordered by dunes or higher areas on almost all sides, the centre of the island is relatively low in elevation. A channel connects the salt marsh in the centre of the island to the Wadden Sea. Changes from 2005 to 2007 were small compared to later years.

The washover system was first visible on the DEM from 2013 (Figure 2.6c), when part of the dunes in the north had eroded to an elevation lower than 3 metres. The remaining dunes had steepened. This can be seen in Figure 2.7a, which shows a transect of the island. The washover also covered an area that had previously been a salt marsh, but the washover had not yet reached its present size. Between 2005 and 2013, the beach expanded for the central part of the island, while the beach in the eastern and western part of the island expanded (Wesselman, 2019).

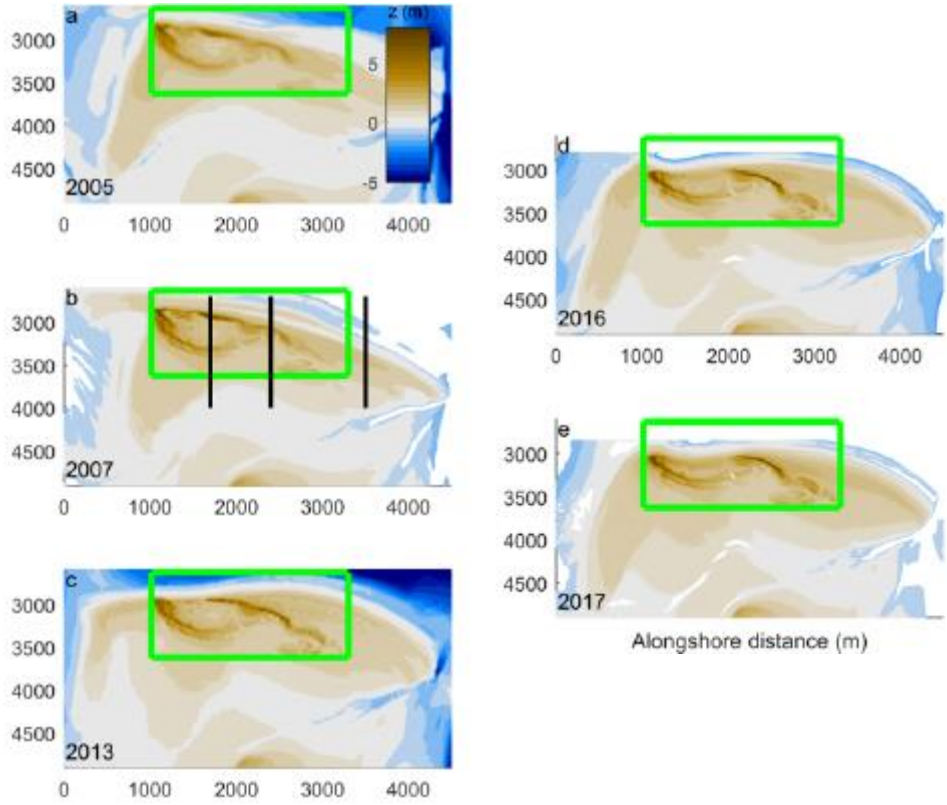

Figure 2.6. Source: Wesselman, 2019. DEMs of Rottumeroog. The black lines in Figure b) indicate the location of the transects shown in Figure 2.7.

Between 2013 and 2016, the washover continued to grow and reached its present size of approximately 600 metres in width (see Figure 2.6d). Most of the remaining dunes were eroded at the expense of the washover. The dune erosion in the central part of the island was compensated

by dune growth in the east of the island, resulting in the dune volume remaining equal. This dune growth in the eastern part of the island is already visible on images from 2007. After 2013, the beach was in retreat over the entire length of the coastline (Wesselman, 2019).

The washover system continued to expand between 2016 and 2017, and the washover accreted up to 0.8 metres vertically (see Figure 2.7d and e). Sedimentation rates per meter of coastline were approximately 60 m^3/m. This rate is similar to sedimentation rates during extreme storms or hurricanes in other parts of the world. Because dune breaching hardly occurred during this period, there must have been another source of sediment. The continuing retreat of the beach and beach erosion indicate that the beach must have been this sediment source. Net sedimentation along cross-shore profiles was found to be approximately zero for the central part surrounding the washover. This also implies that for the central part of Rottumeroog, the sediment eroded from the beach was deposited in the washover (Wesselman, 2019). Wesselman (2019) proposes that smaller deposition volumes in other washovers (for example on Schiermonnikoog; Engelstad et al., 2018) might be linked to the lack of a rapidly retreating beach as a sediment source. In total, the beach retreated 200 metres between 2005 and 2017 (Wesselman, 2019).

High sedimentation rates were also observed at the island tail. Sedimentation rates here are slightly lower than in the washover, but the area is also larger. This indicates that washover opening conditions, such as flow acceleration due to 2D effects, were not present on Rottumeroog as the sedimentation rates are similar. However, the washover is effective in transporting sediment (net erosion was observed landward of the high dunes; Wesselman, 2019).

The coarse temporal resolution of the study by Wesselman (2019) meant that only the general evolution of the washover was studied, while changes on smaller timescales were not observed. It was therefore not possible to determine when the observed changes occurred, and what caused these changes.

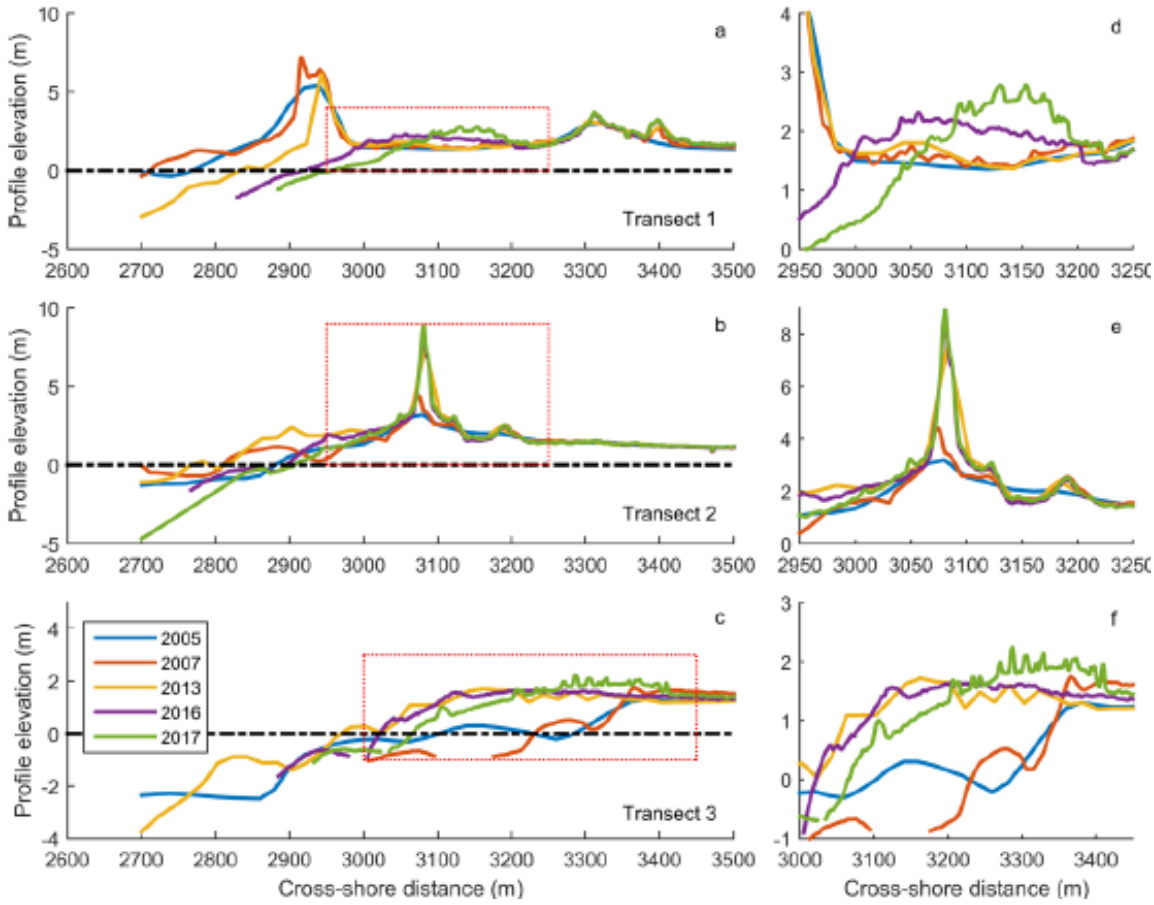

Figure 2.7. Source: Wesselman (2019). 1D transects of Rottumeroog in the cross-shore direction. Transect a) is in the centre of the washover, transect b) is in the eastern part of the island, which experienced strong dune growth, and transect c) is on the island tail. Transects d), e) and f) are more detailed versions of transects a), b) and c).

2.3. Research questions and hypotheses

The washover on Rottumeroog was chosen for this study for several reasons. Firstly, Rottumeroog evolved naturally since 2005, so there is no human interference in the system. Secondly, the recent development of the washover allows the washover to be studied since its inception. Thirdly, the previous research by Wesselman (2019) using DEMs allows for a more in-depth analysis of the washover system.

The following questions are the sub-research questions which will be examined:

What are the multi-year trends in washover evolution?

What are the seasonal trends in washover evolution?

What are the controlling factors in washover evolution?

The spatial resolution of most satellites is too coarse to study washover evolution effectively, as washovers are often relatively small features. Therefore, LiDAR (Aagaard & Kroon, 2019) or aerial photographs (Mathew et al., 2010) are often used. This study has opted for high-resolution satellite imagery, with a spatial resolution of 3 to 5 metres, and a temporal resolution of weeks to months.

The high temporal resolution allows for an analysis on much smaller timescales than what has been studied so far. This allows for both an in-depth analysis of the washover on a multi-year timescale and of an analysis of a washover system on a seasonal timescale, which has not been studied previously. Washover evolution on a seasonal timescale can give an indication of when overwash events occur. The overwash frequency likely influences processes such as embryo dune formation and vegetation recovery. The usage of satellite imagery also allows to study the evolution of vegetation inside a washover, though it does not allow for the study of changes in elevation, which was already studied by Wesselman (2019).

Based on the work on Rottumeroog by Wesselman (2019) and on similar studies, several hypotheses can be formulated. It is expected that the washover formed at some point between 2007 and 2013, likely closer to 2013 than to 2007, because of the speed of the washover expansion in the subsequent years. The subsequent expansion of the washover was already reported by Wesselman (2019), and therefore it is expected that the washover will continue to expand in 2018 and 2019. It is also expected that the island will continue to migrate in the onshore direction.

Given the lack of research into seasonal washover evolution, it is hard to predict how the washover will change on a seasonal scale. It is however expected that there will be a form of seasonal influence as a result of the vegetation cycle and because of seasonal changes in storm frequency. It is expected that washovers will occur predominantly or even solely in winter, which was the case for a washover in Denmark (Aagaard & Kroon, 2019). This implies that washover expansion will also predominantly occur in winter. Washovers will lead to the destruction of foredunes, the removal of vegetation and the deposition of additional sediment, which all lead to an increase in the sand area.

However, vegetation recovery will likely be limited, as overwash leads to a high salt stress, as was reported Nielsen & Nielsen (2006) for a washover in Denmark. It is however possible that the high accretion rates inside the washover result in decreasing the likelihood of overwash, which decreases the salt stress and allows vegetation to colonise.

It is difficult to predict the importance of aeolian processes in the washover as it has received little attention in the past. Wesselman (2019) that processes such as flow acceleration and 2D effects were not present at the washover at Rottumeroog. Therefore, it is likely that these processes also do not occur for wind, in contrast to, for example, blowouts where wind is steered and accelerated (e.g., Hesp & Hyde, 1996). This implies that the magnitude of aeolian transport in the washover is likely comparable to that of a beach. The amount of aeolian transport in the washover will be strongly affected by the wetness of the sand, which is much higher after overwash. It is therefore likely that aeolian transport is lower in winter and higher in summer when the overwash frequency is lower.

3. Methods

The imagery used was obtained from Planet Labs, Inc, a private company which collects high-resolution imagery using a large number of mini-satellites. Imagery from two satellite systems was used: PlanetScope and RapidEye. PlanetScope images are collected in the in the RGB (red, green and blue) and NIR (near-infrared) bands and have a spatial resolution of 3 metres. PlanetScope has been active since mid-2016. Because of the large number of satellites, PlanetScope imagery has an extremely high temporal resolution, up to several images a week. RapidEye images are collected in the RGB, red edge and NIR bands and have a spatial resolution of 5 metres. Table 3.1 shows the spectral bandwidths for both satellite systems. The RapidEye satellites were first launched in 2008. The RapidEye constellation contains fewer satellites and therefore has a lower temporal resolution.

The period studied ran from the 30th of June 2009, when the first satellite image was available, to the 29th of October 2019. As PlanetScope imagery has a higher spatial and temporal resolution, PlanetScope imagery was preferred over RapidEye. This meant that RapidEye imagery was used before October 2016, while PlanetScope was used from October 2016 onwards.

Band	PlanetScope wavelength (nm)	RapidEye wavelength (nm)
Blue	455-515	440-510
Green	500-590	520-590
Red	590-670	630-685
Red Edge	-	690-730
NIR	780-860	760-850

Table 3.1. Spectral bandwidths of the PlanetScope and RapidEye satellite systems.

Analytic (multispectral) data was the primary type of imagery used, but visual imagery was used as supporting data. The downloaded imagery had been orthorectified, with a RMSE of <10 m, and the PlanetScope imagery had been scaled to surface reflectance using a radiative transfer code, and MODIS NRT data. The RapidEye imagery had not been scaled to surface reflection, instead displaying absolute radiometric values based on calibration coefficients (Planet, 2019).

3.1. Pre-processing

The following section will describe the workflow that was used to download, process and analyse the satellite imagery. A simplified version of this workflow is shown in Figure 3.1. First, a virtual environment was made in Python using Anaconda Prompt. This environment was linked to Planet by installing a package called planet, which can be installed in Anaconda Prompt. To download the images, a tool (porder) was used (Roy, 2019). porder and associated tools were downloaded and installed in the virtual environment. This allowed to create an id-list containing a large amount of images, based on certain parameters. These parameters include the date range,

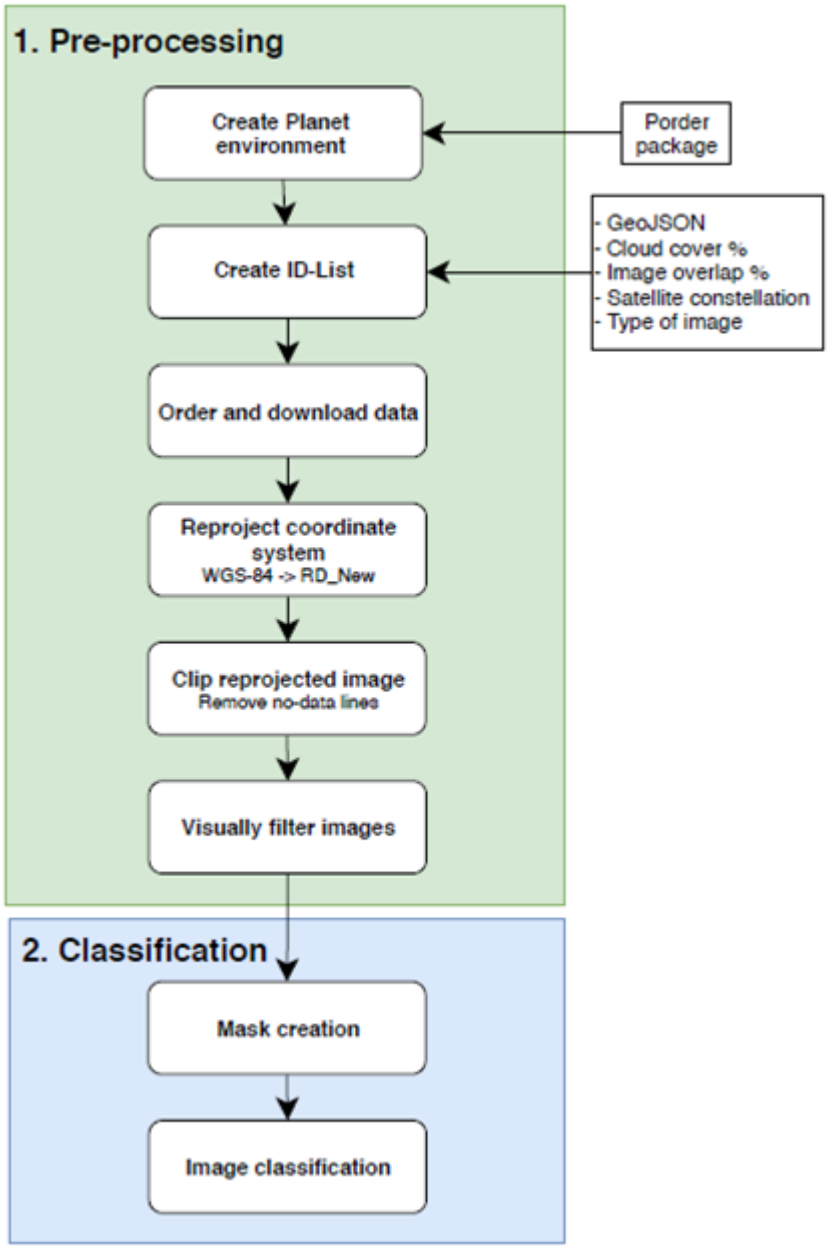

Figure 3.1. Adapted from: Maas (2020) and Schemmekes (2020). Workflow that was used to download and analyse the imagery from Planet.

the satellite constellation, the type of image (visual or analytic), the maximum cloud cover percentage (set at 40%) and the overlap with a predefined area. This area was defined in a .geojson file which was used to define the boundaries of the study area. The .geojson file defined an area around Rottumeroog of about 3 by 1.4 km. This id-list can then be used to download the images. When running the commands to download the images, an error message appeared. This happened on several devices and no cause was found. This problem was circumvented by copying an installation folder from (Maas, 2020).

After the images were downloaded, they were converted from UTM WGS84 to the Rijksdriehoeksstelsel (RD), a Dutch coordinate system. Afterwards, the images were clipped to

remove the areas along the borders of the image, which had missing data after the conversion to RD. For this, two programs (reproject.bat and clipNotches.bat) were used (provided by B.G. Ruessink).

Not all images were perfectly aligned with each other. This would influence the (pixel-based) classification. The images which had moved to such an extent that a large part of the island was missing, were deleted, while images which had moved a few pixels were *registered*, i.e. moved to the correct position. This was done manually in Matlab by comparing the moved image to an image which was in the correct spatial position (Maas, 2020), using the Control Point Selection Tool. This tool does not support multispectral images. Therefore, the bands of the images were extracted and transformed into a greyscale image, which was then registered, after which the individual bands were moved in the same manner as the greyscale image. The bands were then reassembled to create a new image. This assumes that the different bands were correctly positioned relative to each other. The manual registration of images was difficult because of the absence of fixed points such as roads or buildings on Rottumeroog. Although the image registration moved the images closer to the correct position, this was almost never perfect, resulting in a slight error of ~1-2 pixels. Because this procedure was labour-intensive, it was not carried out when the data availability was good (multiple images a week), in which case moved images were deleted instead of registered.

After the images were processed, they were manually checked if they did not contain any clouds, snow or errors, such as faulty data. If there were multiple images from the same day, only one of the images was kept. The number of images available per month and per year can be seen in Figure 3.2. As cloud cover is typically high during the winter and low during the summer, there are much fewer available images during the cloudier months, approximately from October to March) than during the less cloudy months (approximately from April to September). The amount of images greatly increases from October 2016 onwards, when the PlanetScope imagery becomes available. The amount of available RapidEye imagery fluctuates greatly, ranging from 2 images in 2016 to 9 in 2015.

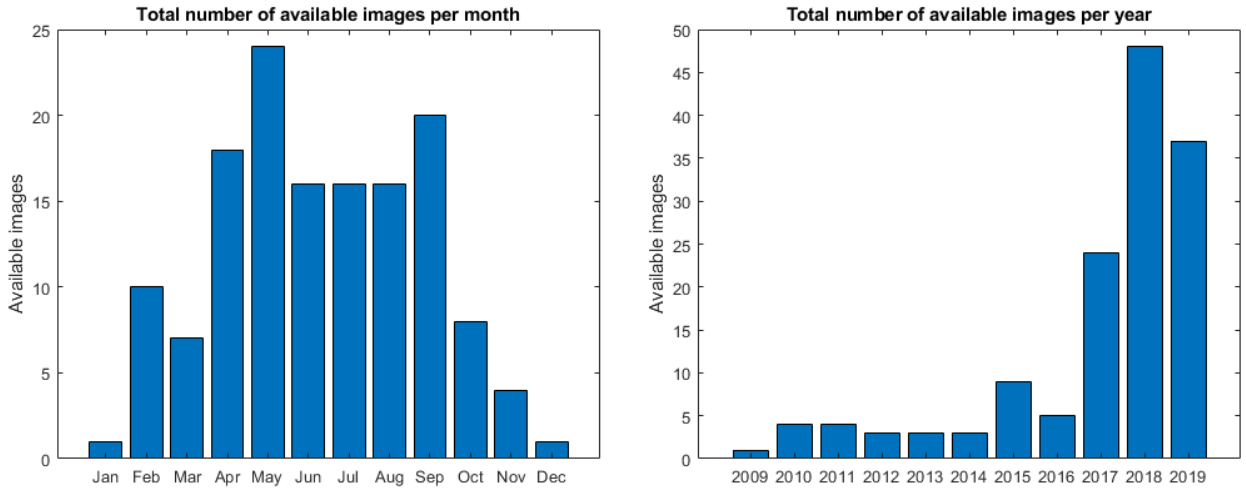

Figure 3.2. Distribution of the total number of available images per month (left) and year (right), after images were manually checked for clouds, incorrect data, etc.

3.2. Classification

The image analysis itself was performed in Matlab. The scripts for image classification and analysis were mostly taken from another research (Schemmekes, 2020; Maas, 2020), but were adjusted for the situation at Rottumeroog. They were also further adjusted and expanded, for example by making time-dependent classifications.

First, masks were created, which set the pixel values in the area covered by the mask to zero. The masks covered all areas except for the washover and its immediate vicinity, so that changes in the area reflect changes in the washover and not changes elsewhere, and to minimise the noise and the uncertainty resulting from the classification. The sea was also excluded as the fluctuations in water level (resulting from e.g. the tides) would result in large changes in the classification. As the island moved southward over time, different masks were needed as different areas had to be masked: three for the RapidEye images and one for the PlanetScope images. The first mask was used from 2009 to 2011, the second mask from 2012 to 2014, the third mask from 2015 until mid-2016. The fourth mask was used for the PlanetScope images (from mid-2016 onwards). The location of these four masks is shown in Figure 3.3. The total area of the unmasked region was 359676 m^2 for the PlanetScope imagery. In certain situations, different masks were created to investigate those specific situations.

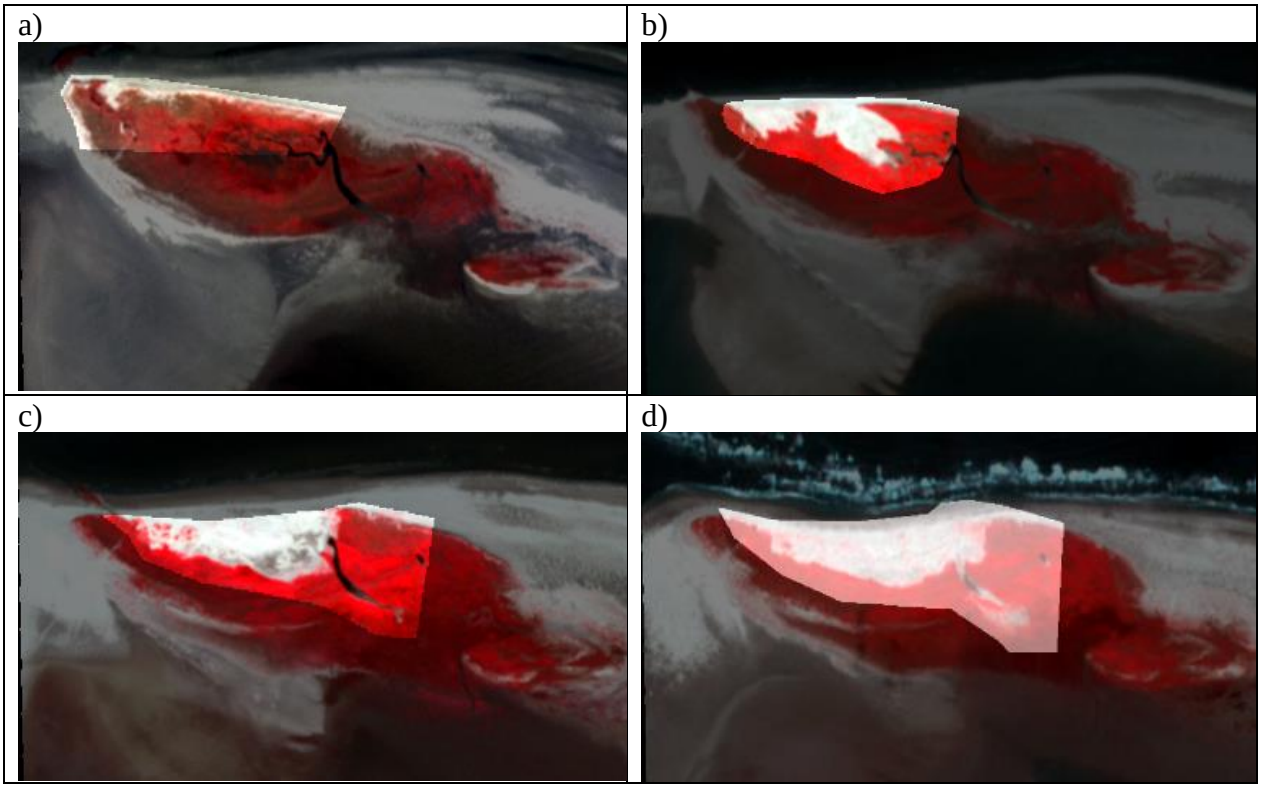

Figure 3.3. Location of the four primary masks used. The darker areas are the masked areas.
a) Mask for 2009-2011. b) Mask for 2012-2014. c) Mask for 2015-mid-2016.
d) Mask from mid-2016 onwards (PlanetScope imagery).

After the masks were created, the pixels were classified using a pixel-based classification method which classifies the pixels in three classes: vegetation, sand and water. The variables used in the formulas used to classify pixels were found iteratively, but were based on the spectral characteristics of sand, vegetation and water. Pixels were classified as vegetation when the Normalised Difference Vegetation Index (NDVI) was larger than a variable times the Otsu threshold, while the remaining pixels were classified as sand. The NDVI is an indicator for the presence of vegetation in a pixel, and is calculated using the following formula:

$$\mathrm{NDVI} = \frac{(\mathrm{NIR} - \mathrm{Red})}{(\mathrm{NIR} + \mathrm{Red})}$$

The Otsu threshold is a threshold created by an unsupervised classification, which separates an image into two classes so that the separability between these classes is maximised (Otsu, 1979). As the vast majority of pixels in the image were either vegetation or sand, this method worked well to separate these two classes. As the Otsu threshold and the average reflection in a certain band are specific to each image, these can be used to successfully classify different images, without having to find new parameters for each image (Schemmekes, 2020; Maas, 2020).

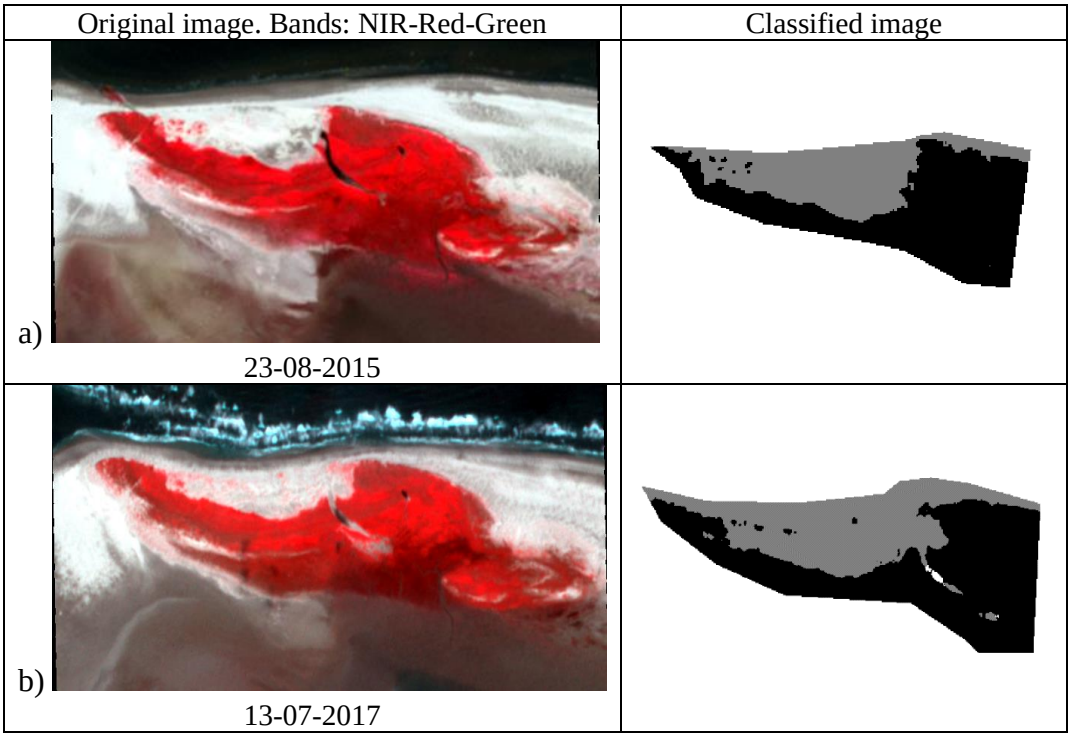

Figure 3.4. a) Original false colour image (RapidEye) and the classified image for 23-08-2015. b) Original false colour image (PlanetScope) and the classified image for 13-07-2017. In the top images, the NIR band is shown as red, causing vegetation to appear red. In the classified images, only the unmasked pixels have been classified. Vegetation is coloured black; sand is coloured grey and water is coloured white. As no water class was classified for the RapidEye images, the water pixels in the channel are instead classified as water.

Pixels could also be classified as water when the NDVI was lower than a variable times the Otsu threshold, and when the reflection in the blue band was lower than average. The 'water' class does not represent the sea, which had been masked out, but inland bodies of water. In images where the sea level was high enough to enter the unmasked area, the sea pixels were manually classified as sand, because classifying them as water would result in large fluctuations in the area covered by each class. There were problems with the classification of the water class for the RapidEye imagery. The coarser resolution made it more difficult to recognise water pixels, and the sensitivity of the classification towards water pixels varied greatly. This resulted in the amount of water pixels to be often either greatly overestimated or underestimated, compared to a visual inspection of the RGB image. Therefore, it was decided not to use the water class for RapidEye imagery. An example of this classification is given in Figure 3.4.

3.3. Additional data

Additional data was used to support the analyses made. The additional data include water levels, the significant wave height, wind data and weather data. The water levels were obtained from Rijkswaterstaat, for the Huibertgat, which lies about 10 kilometres to the northwest of Rottumeroog. Figure 3.5 shows the average maximum water level for each month between 2009 and 2019. The mean maximum water levels are highest from October to January, and lowest from April to August.

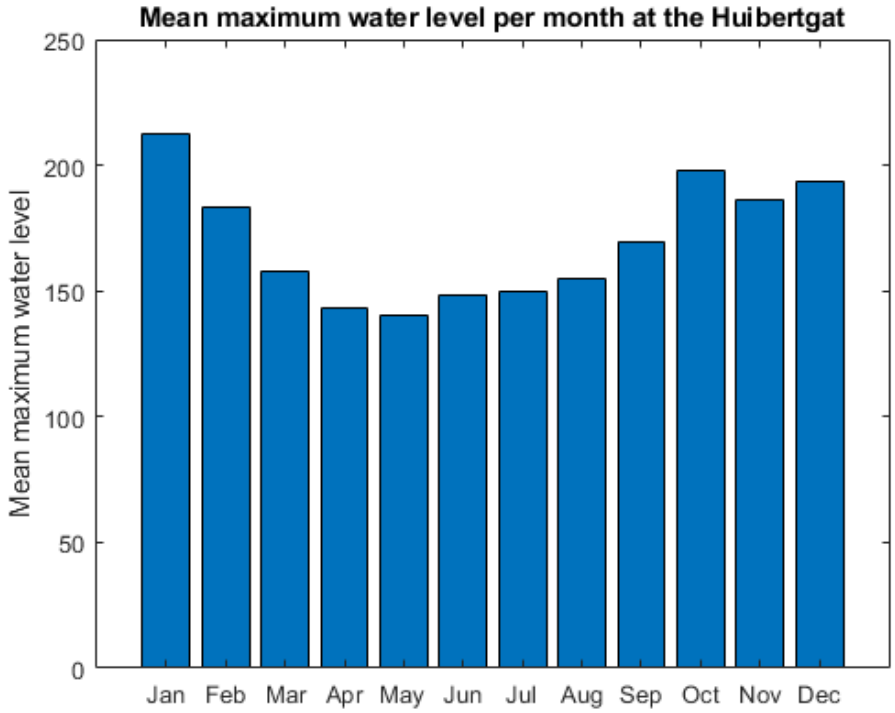

Figure 3.5. The maximum water level per month, averaged from 2009 to 2019. Water levels are with respect to the NAP (Nationaal Amsterdams Peil; the Dutch national vertical datum).

The significant wave height H_s was obtained from Rijkswaterstaat from the Westereems Oost buoy, almost 10 kilometres to the north-north-west of Rottumeroog. Figure 3.6 shows a

timeseries of the significant wave height. The significant wave height varied considerably, with a maximum of 6.78 metres. Both the water level and the H_s dataset contained a few periods with missing data but were mostly complete.

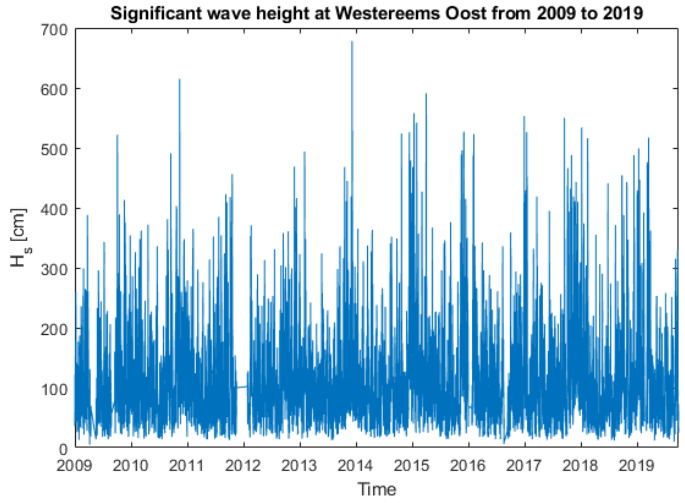

Figure 3.6. The significant wave height H_s at the Westereems Oost buoy from 2009 to 2019.

Temperature and precipitation data was obtained from the KNMI for the Lauwersoog station. A timeseries of the maximum, minimum and mean temperature for each month is shown in Figure 3.7. The average temperature varies between 0 and 5 ºC in winter and 15 and 20 ºC in summer. The precipitation distribution is shown in Figure 3.8a, which shows the cumulative precipitation per month. Figure 3.8b shows the cumulative precipitation per year, and Figure 3.8c the average precipitation per month. The annual precipitation ranges from 620 mm/year to 986 mm/year. The average monthly precipitation peaks with 84 mm in August and remains high until December, while the precipitation is low from February to April, with a minimum of 40 mm in April.

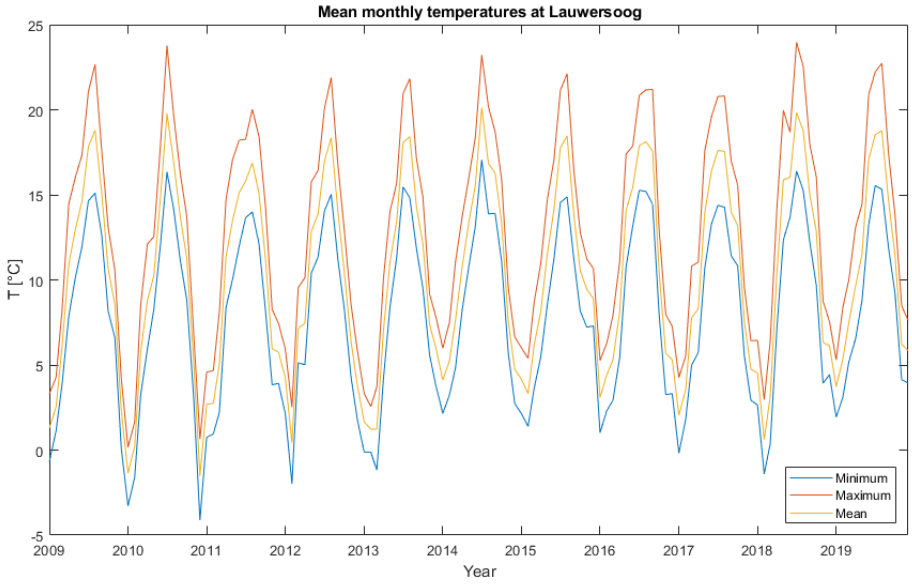

Figure 3.7. Mean monthly maximum, minimum and average temperatures at Lauwersoog.

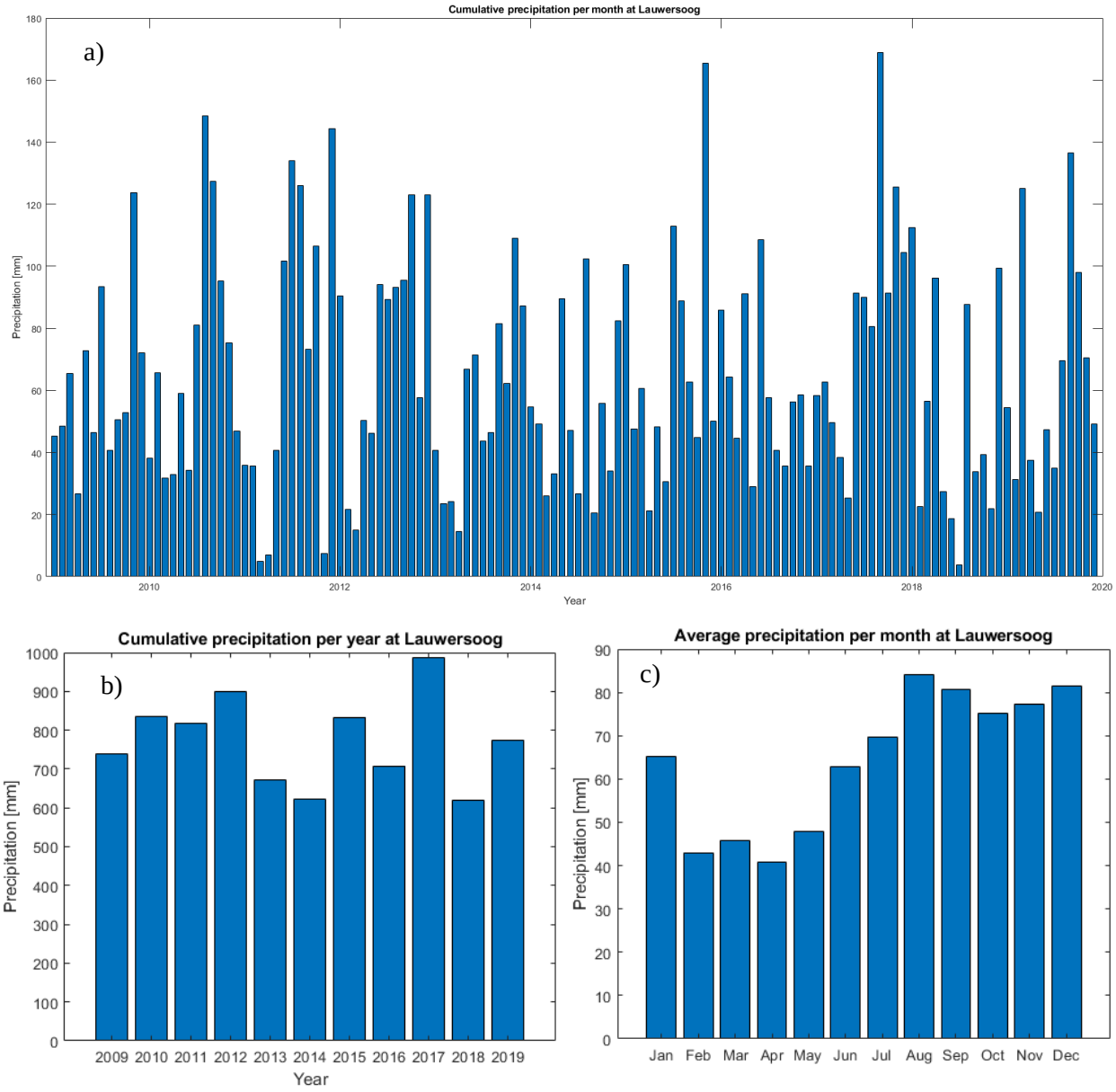

Figure 3.8. a) Cumulative precipitation data for each month from 2009 to 2019, b) Cumulative precipitation data for each year from 2009 to 2019, c) Average monthly precipitation per month

Hourly wind data containing the wind speed and direction was obtained from the KNMI for the Huibertgat station. Wind roses were made using a script in Matlab (Pereira, 2015). Figure 3.9 shows a wind rose for the Huibertgat station. The prevailing wind direction is from the southwest, with winds form the west or northwest being slightly less common. Winds from the north are very uncommon. For easterly winds, winds from the northeast are the most prevalent. As the data from the Huibertgat station was incomplete, wind data from the Lauwersoog station, about 30 kilometres to the southwest of Rottumeroog, was used if there was no data from the Huibertgat available.

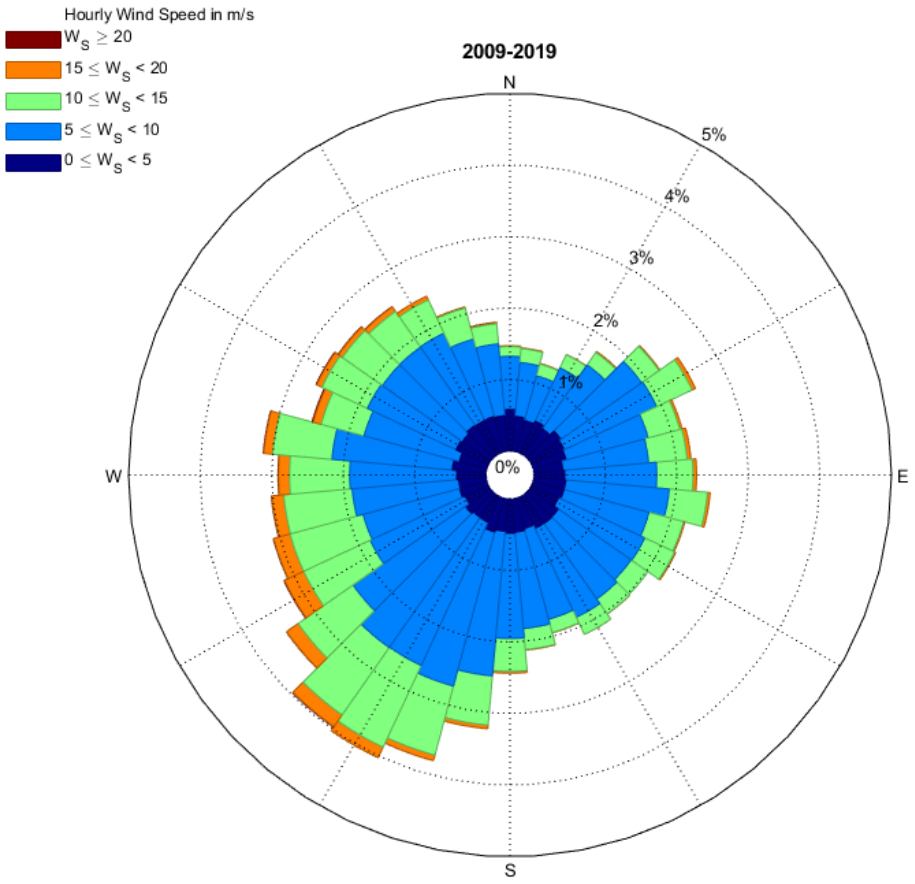

Figure 3.9. Wind rose showing the frequency of different wind speeds at the Huibertgat. The percentages indicate the frequency of winds blowing from that direction.

4. Results

The results are presented in three sections. The first two sections will exclusively focus on the analysis of the classified images. The first and the second section will discuss the seasonal and the long-term trends respectively, focusing on vegetation and sand cover, as these classes together constitute the vast majority of pixels. Afterwards, the relation between washover development and the forcing conditions is considered through the comparison between the classified images and the supporting data.

4.1. Seasonal trends:

The washover shows a strong seasonal variation, as can been seen in Figure 4.1. Figure 4.1d shows the area covered by vegetation in and around the washover, from October 2016 to October 2019, in the unmasked areas of the image. There is a clear seasonal trend, with vegetation occupying a larger area in summer than in winter. An example of this can be seen in Figure 4.2. The vegetated area typically peaks between September and November, after which it declines to a minimum in April or May. Afterwards, the vegetated area increases again. The maximum vegetation cover is significantly lower in 2018 than in the other years, while the minimum vegetation cover remains approximately the same. The same trends are visible in Figures 4.4a and b, which show the area covered by vegetation from 2009 to 2014, though the exact month in which the vegetated area peaks cannot be determined because of a lack of data. Note that the vegetated area in the different subplots cannot be compared directly because different masks were used. Also, the variation in Figure 4.1a is extremely small. Figure 4.1c, which shows the area covered by vegetation from 2015 to mid-2016, shows a slightly different trend. Instead of peaking between September and November, the area covered by vegetation already peaked in July, resulting in a low peak in vegetation cover. The further evolution of the vegetated area is difficult to follow until April 2016, when the vegetated area has slightly declined.

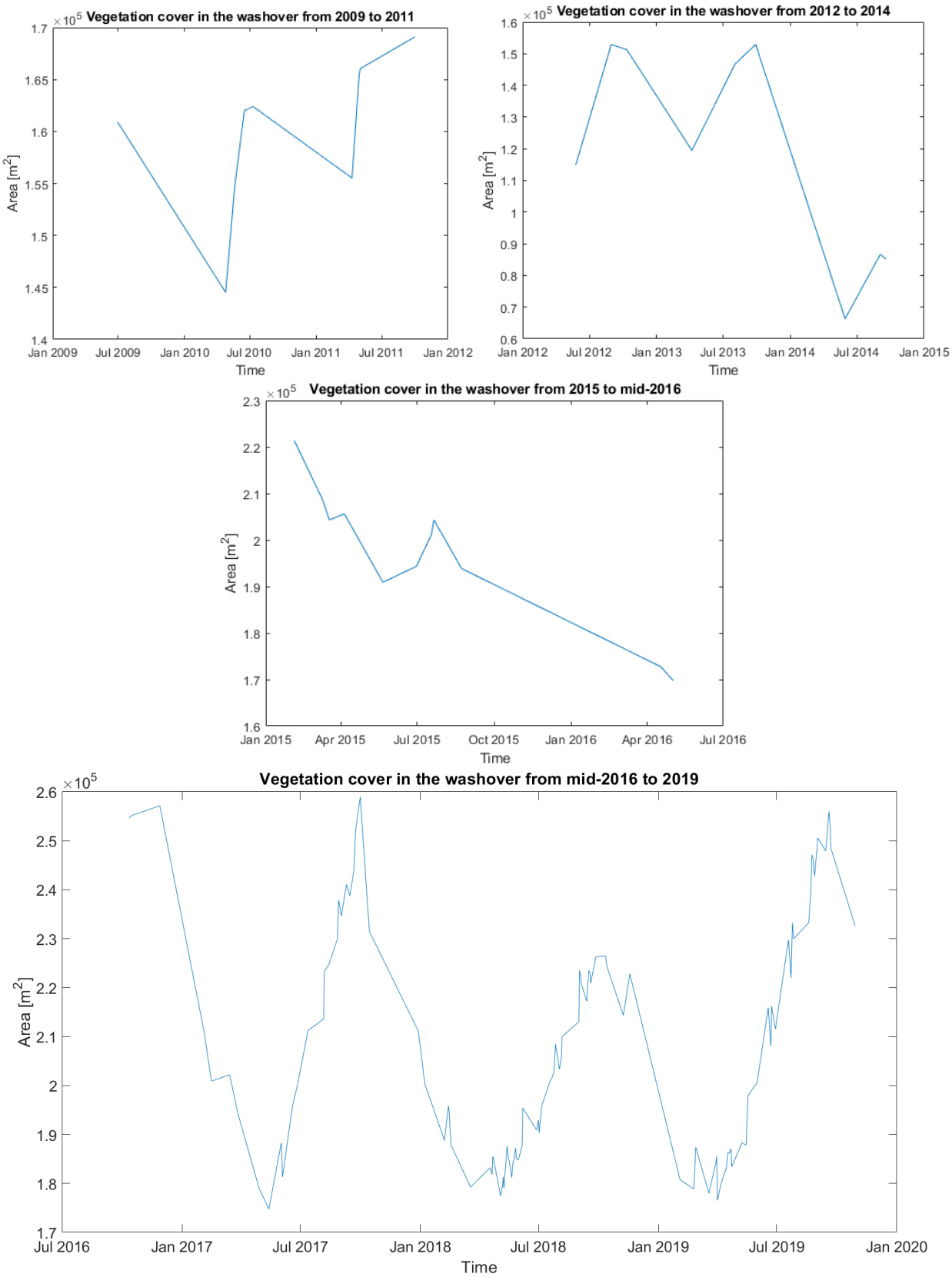

Figure 4.1. Vegetation cover in the washover for selected time frames. A different mask was used for each time frame.

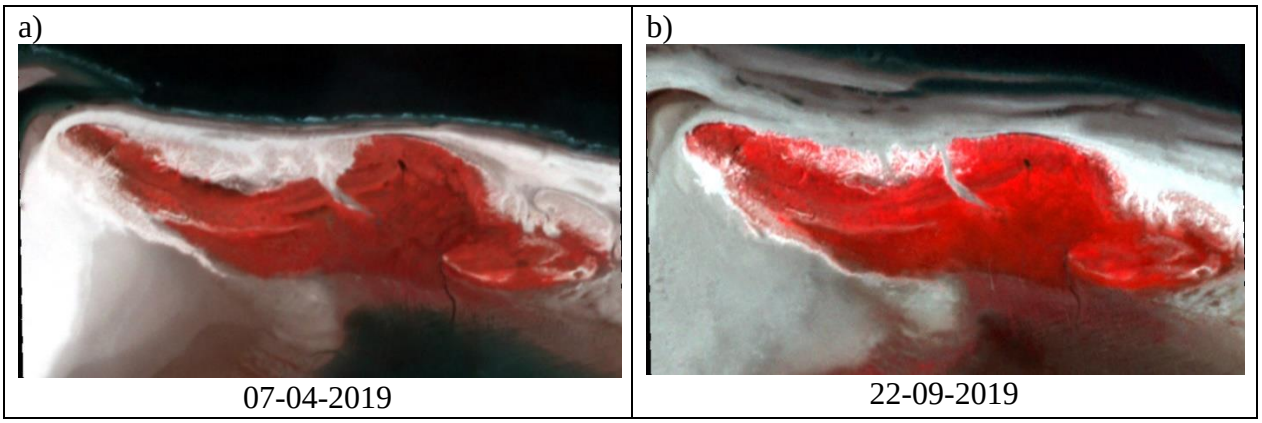

Figure 4.2. False colour (NIR-Red-Green) images in 2019, an example of seasonal variation with a lower vegetation cover in April than in September.

Figure 4.3 shows the difference between the maximum and minimum vegetation cover in a year. This approximates the area which is vegetated for part of a year, an indication of the amount of seasonal variation. This area is relatively low at first, between $1.3 \cdot 10^4$ and $1.7 \cdot 10^4$ m^2 in 2010 and 2011. In 2012, the area greatly increases to $3.8 \cdot 10^4$ m^2. In the following years, it declines to a minimum of $1.3 \cdot 10^4$ in 2015. In 2016, it increases to $8.7 \cdot 10^4$ m^2, an increase of 651%. It remains relatively constant in the following years, with the exception of 2018, when it decreases by approximately 42%.

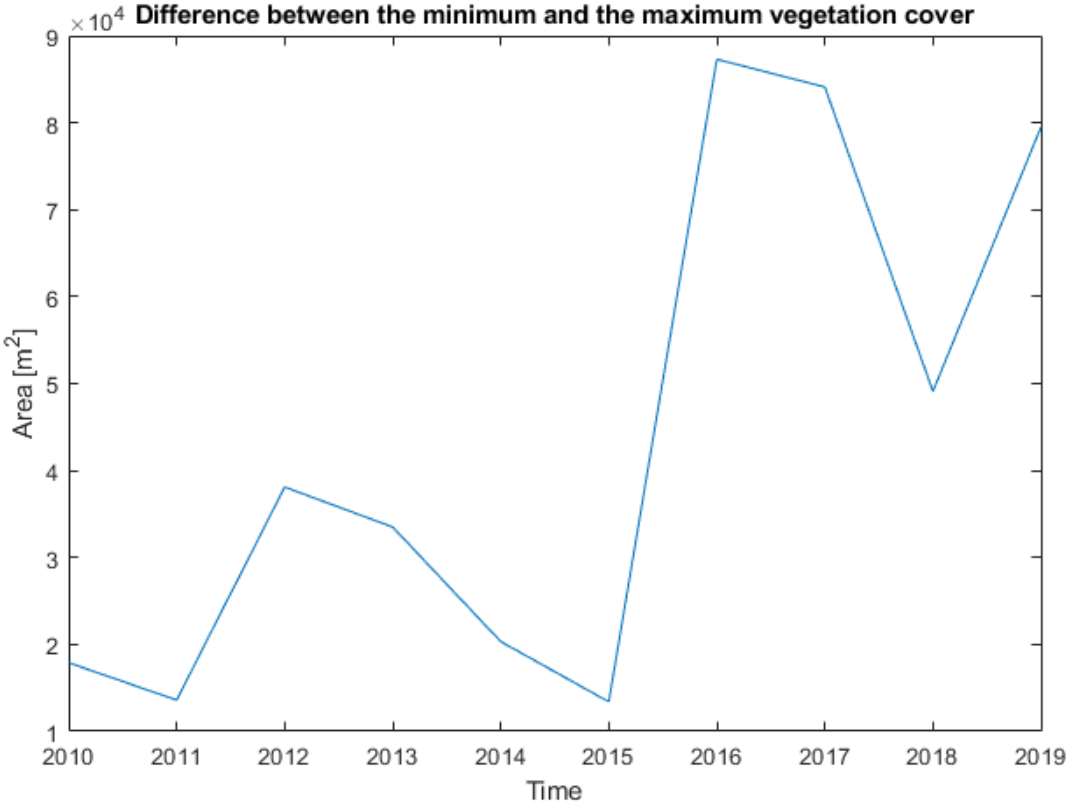

Figure 4.3. The difference between the minimum and the maximum vegetation cover in a year.

When the difference between the maximum and minimum vegetation cover is expressed as a percentage of the area of the washover (the maximum sand area for a given year), the trend changes, as can been seen in Figure 4.4. In 2010 and 2011, the difference between the maximum and minimum vegetation actually exceeds the area of the washover. After 2011, the percentage ranged from 13% in 2015 to 85% in 2019, following a similar trend as the absolute change. There is a sudden increase from 13% in 2015 to 70% in 2016, and a marked decrease from 71% in 2017 to 35% in 2018.

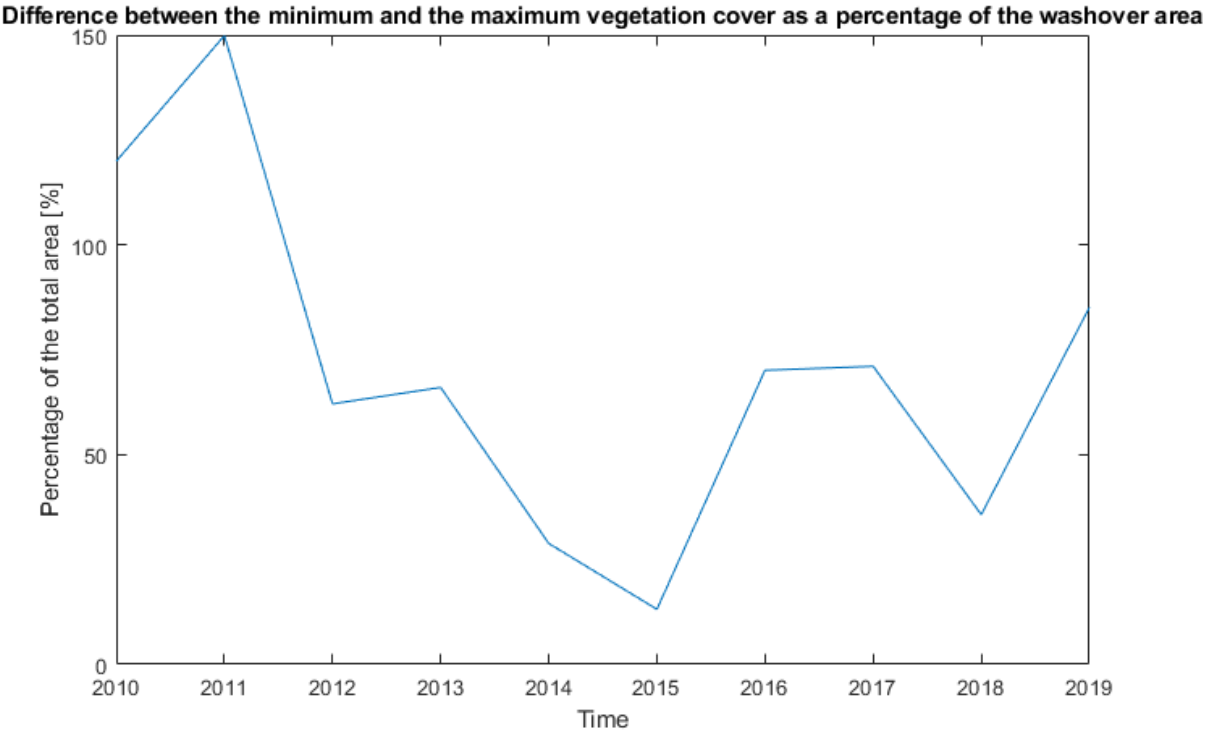

Figure 4.4. The difference between the minimum and the maximum vegetation cover in a year as a percentage of the total area of the washover. The percentages higher than 100% are likely a cause of the different masks used to determine the two different areas.

Figure 4.5 shows a map with the percentage of time that a pixel is classified as vegetation between October 2016 and 2019. The yellow areas are almost always vegetated while the dark blue areas are almost never vegetated. The colours in between indicate areas which are vegetated in certain images but not in others. These colours therefore either indicate seasonal or permanent changes. The outline of the washover is clearly visible as a large, mostly unvegetated area, with an unvegetated area to the north (the beach), but otherwise surrounded by vegetated areas. At the western side of the washover, the contour lines form several patches, with more frequent vegetation cover in the middle of the patch than at the sides. These patches are mostly absent from the central and eastern part of the washover. In the central part of the washover, vegetation cover frequency mostly increases from north to south, while in the eastern part, it increases both from north to south and from east to west. The channel is almost never vegetated. In the central

part, the contour lines are often relatively close together, while in the eastern part, they are often further apart, indicating that this area experiences greater variation.

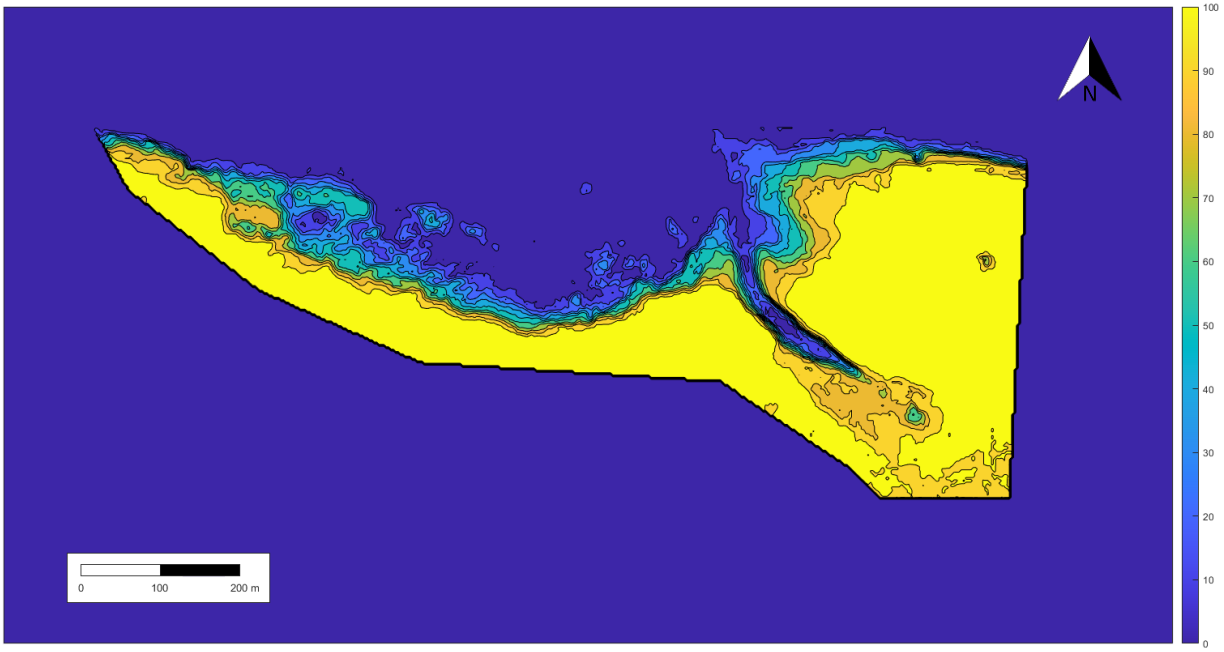

Figure 4.5. Spatial distribution of the percentage of time that a pixel is classified as vegetation from October 2016 to October 2019.

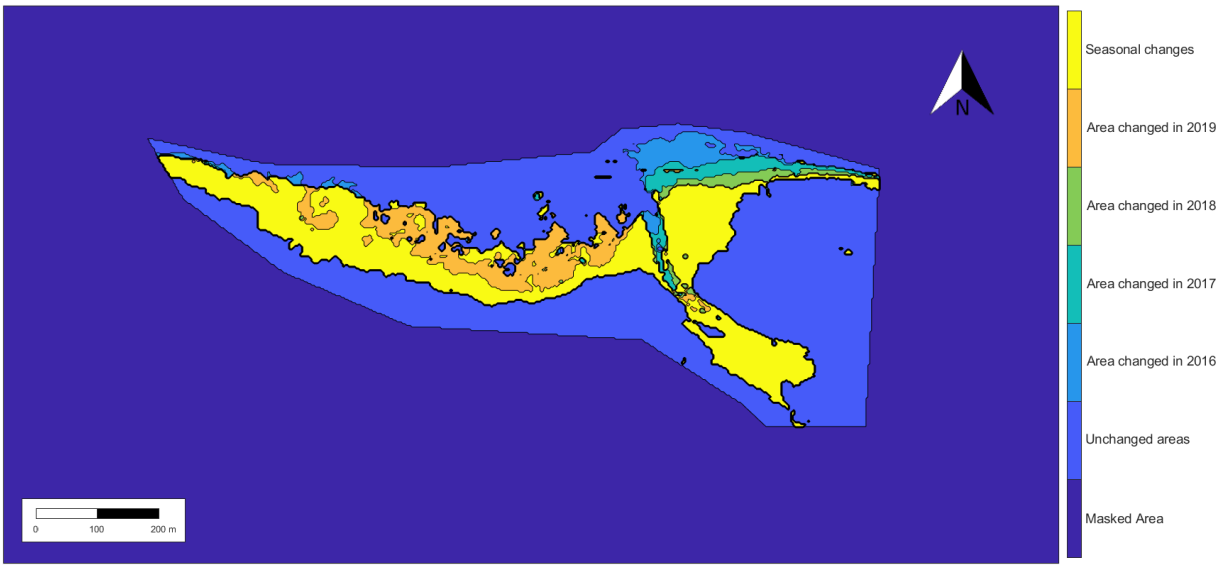

Figure 4.6. Map showing the type of change in classification from October 2016 to October 2019. The changes shown are the changes between the minimum and the maximum vegetation cover for each year, starting with the maximum vegetation cover in late 2016, and ending with the maximum vegetation cover in mid-2019. The areas with seasonal changes have experienced an even number of changes between late 2016 and 2019, while the areas changed in a certain year denote areas which have experienced an odd amount of changes, denoting permanent changes. These areas are classified by the year in which they last changed.

Figure 4.6 shows a map showing whether the observed changes in the washover are seasonal or permanent by comparing the image with the highest vegetation cover in a year with the image with the lowest vegetation cover. Seasonal changes are north of the permanently vegetated area and comprise the majority of pixels which sometimes belong to one class and sometimes to another, as can be seen by comparing Figures 4.8 and 4.9. The area which experiences seasonal change is largest in the eastern and the western part of the washover, and smallest in the centre of the washover. Permanent changes mostly occurred to the north-east of the washover, where a large area shows permanent change. The northernmost area last changed in 2016, the middle area last changed in 2017 and the southernmost area last changed in 2018. A few small areas which last changed in 2016 can be found just northward of the area which experiences seasonal variation in the western part of the washover. These areas all changed from vegetation into sand. The area last changed decreases from $1.1 \cdot 10^4$ m^2 in 2016 to $5.2 \cdot 10^3$ m^2 in 2018. The area changed in 2019 is found at the boundary between the area which experiences seasonal change and the beach, mostly in the central part of the washover. This area consists of sand pixels which changed into vegetated pixels in 2019. The year in which pixels last changed varies for the former channel in the southeast, and no clear pattern is visible, but seasonal patterns appear to be absent from most of the channel, even though the surrounding area is affected by seasonal changes. Much of the seasonal variation southward of the channel can be explained by a temporary expansion of the sand cover in that area in early 2017, which disappeared later that year.

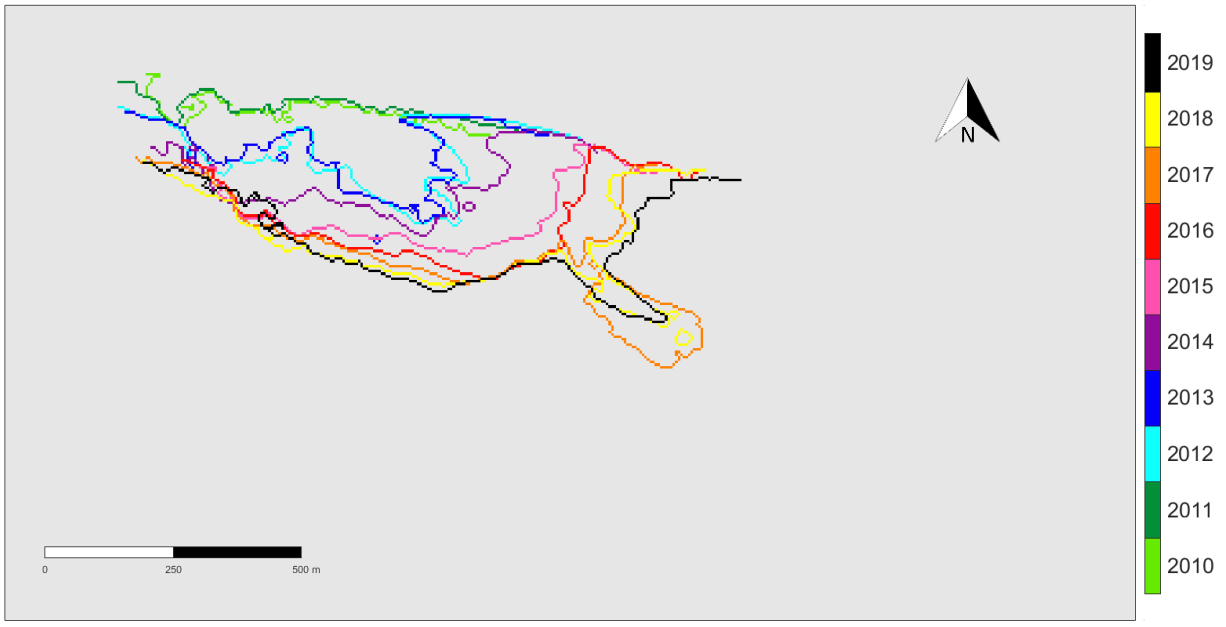

Figure 4.7. Evolution of the boundary between the vegetated area and the non-vegetated area when the sand cover is at its maximum extent for each year (typically in April or May). The vegetated area is to the south of the lines while the non-vegetated area is to the north.

4.2. Long-term trends:

Figure 4.7 shows the boundary between the vegetated and the unvegetated area for different years when the sand cover is at its maximum extent, to minimise the effect of seasonal variation. Therefore, Figure 4.7 gives an indication of the extent of the washover over time. The area south of the line is vegetated while the area north of the line is not. The washover is considered to be the unvegetated area south of an imaginary line between the northernmost vegetated points, while the unvegetated area to the north of this line is part of the beach. Since 2010, the washover has migrated, mostly towards the south. The washover has also expanded, mostly towards the southeast. In 2010 and 2011, the washover is very small as the boundary between the vegetated and the unvegetated area is mostly straight, and the washover is formed by two unvegetated areas protruding in the west (see Figure 4.7 and 4.2a). A particularly strong migration occurred from 2011 to 2012, as the most landward position of the washover in Figure in 2011 is equal to the most seaward position of the washover in 2012 in Figure 4.7, and the washover is also considerably more east in 2012 than in 2011. In 2012, the unvegetated area of the washover consisted of a small but wide area in the west and a large but narrow area in the east, with a south-easterly orientation (see Figure 4.8b). In contrast to the migration and expansion of the washover from 2011 to 2012, there appears to have been very little migration and expansion of the washover from 2012 to 2013. In the following year, the washover both expanded and migrated southward, mostly in the west of the washover. This resulted in the two areas of the washover becoming connected, forming one wide, unvegetated washover (see Figure 4.8c). The southward migration slowed down in 2015 for the western part of the washover and in 2017 for the central part of the washover. The southward expansion of the washover generally continued until the washover reached the dune row in the south of the island (see Figure 2.6). In total, the boundary between the vegetated and the unvegetated area retreated about 150 to 200 metres directly west of the washover, while the retreat was about 300 to 350 metres for the washover itself. The eastward expansion of the washover appeared to have slowed down from 2017 to 2018 but picked up again in 2019 (see Figure 4.8d). From 2016 to 2017, the washover expanded into the channel which previously connected the centre of the island to the Wadden Sea. The extent of the washover in the channel was greatest in 2017, when the sand area was greater in the southern part of the channel and decreased in 2018 and 2019, as it receded from the southern part of the channel.

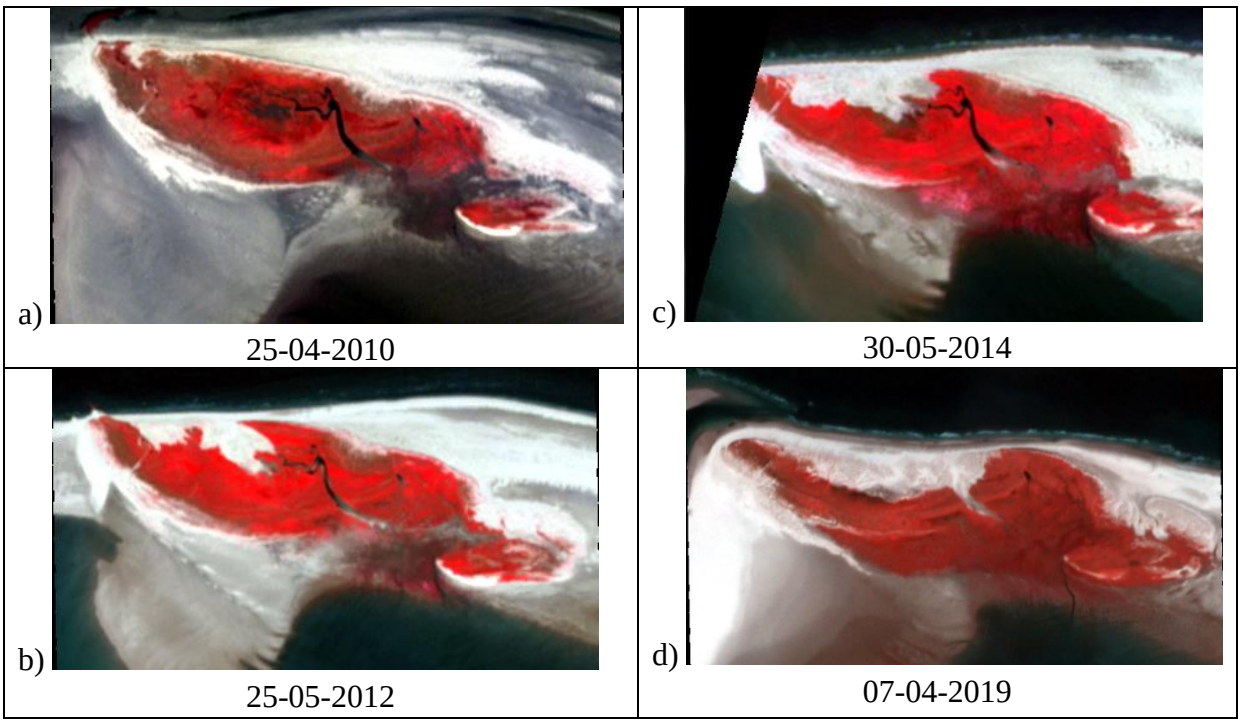

Figure 4.8. False colour (NIR-Red-Green) images of the washover at various points in time.

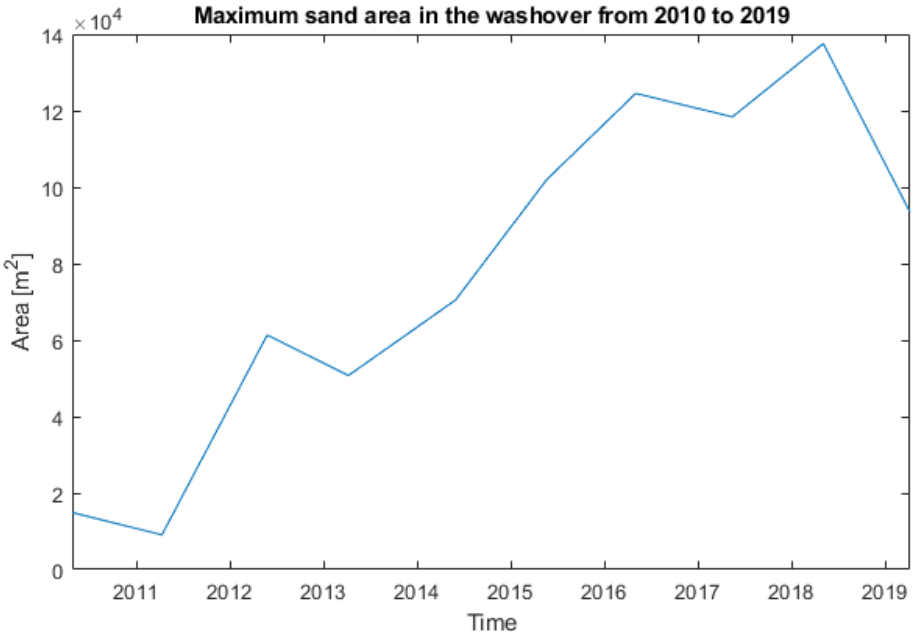

Figure 4.9. The evolution of the maximum sand area in the washover. The maximum sand area is the maximum surface area of the sand inside the washover for a year, which is assumed to be an indication for the size of the washover.

The expansion of the washover is quantified in Figure 4.9, which shows the evolution of the maximum sand area in the washover for a certain year, between 2010 and 2019. The seaward

boundary of the washover was assumed to be a line between the most seaward vegetated pixels directly east and west of the washover, excluding the beach. Therefore, the maximum sand area is assumed to be an indication for the size of the washover. The maximum sand area is relatively small at first, $1.5 \cdot 10^4$ m^2 in 2010. A large large increase to $6.1 \cdot 10^4$ m^2 occurs in 2012. This is followed by a small decrease in 2013. The following years are marked by a strong increase to $1.2 \cdot 10^5$ m^2 in 2016, after which it declines again in 2017. The maximum sand area peaks at $1.3 \cdot 10^5$ in 2018, which is caused by a reduction of the vegetated area in the west of the island, which temporarily shifts the boundary of the washover westward. This peak is followed by a decline to $9.3 \cdot 10^4$ m^2 in 2019. Overall, the maximum sand area shows a strong increasing trend, increasing more than 1500% between 2011 and 2018, indicating washover expansion.

As the vast majority of pixels are classified as either vegetation or sand, a decrease in vegetated area usually corresponds to an increase in sand area. However, parts of the washover are covered by water at certain moments, as can be seen in Figure 4.10. The area covered by water greatly fluctuates, but it is generally high in autumn and winter and low to zero in summer. Unlike the gradual trends in sand and vegetation cover, the water cover typically suddenly increases.

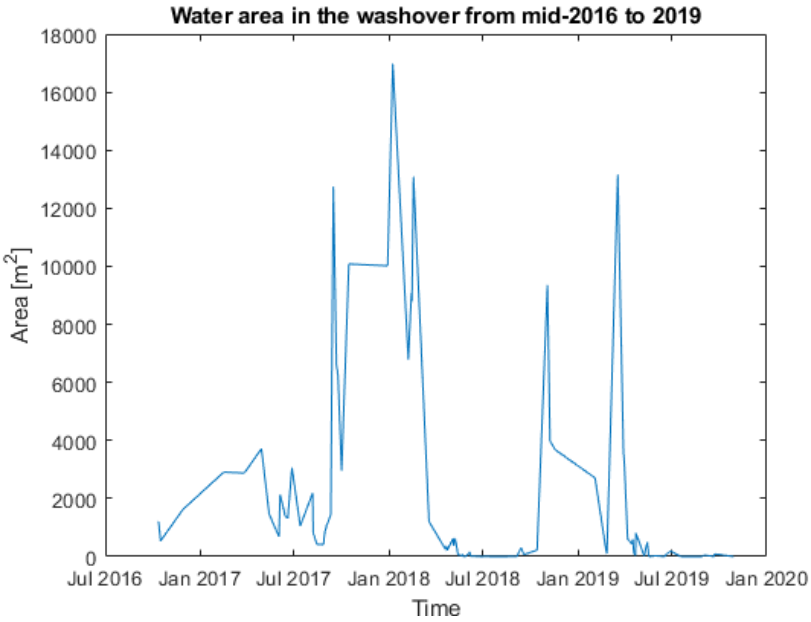

Figure 4.10. Water cover from October 2016 to October 2019.

The percentage of time that a pixel is classified as water is shown in Figure 4.11. There are two areas with a high water cover occurrence: One in the south of the central part of the washover (the western area with a high frequency of water coverage in Figure 4.11), and the other is in the channel in the southeast (the eastern area with a high frequency of water coverage in Figure 4.11). For reference, these areas can also be seen in Figure 4.12a, which shows a satellite image with water cover in these two areas. Overall, the body of water in the channel has

a much higher frequency of water cover than the body of water in the central part of the washover, which is more intermittent.

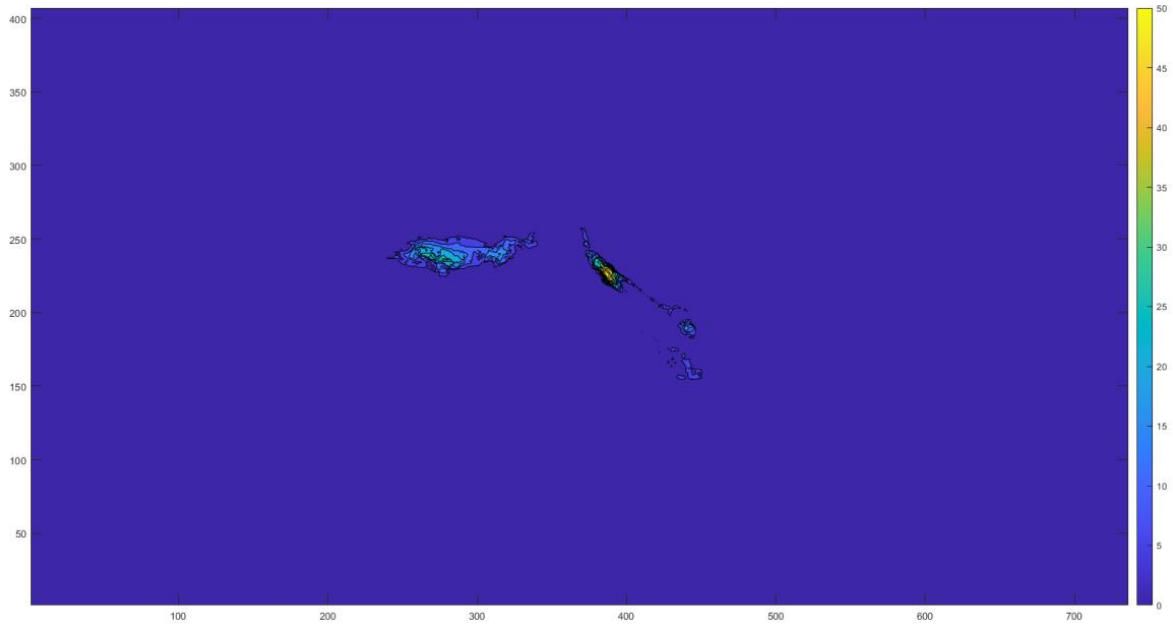

Figure 4.11. Spatial distribution of the percentage of time that a pixel is classified as water from October 2016 to October 2019.

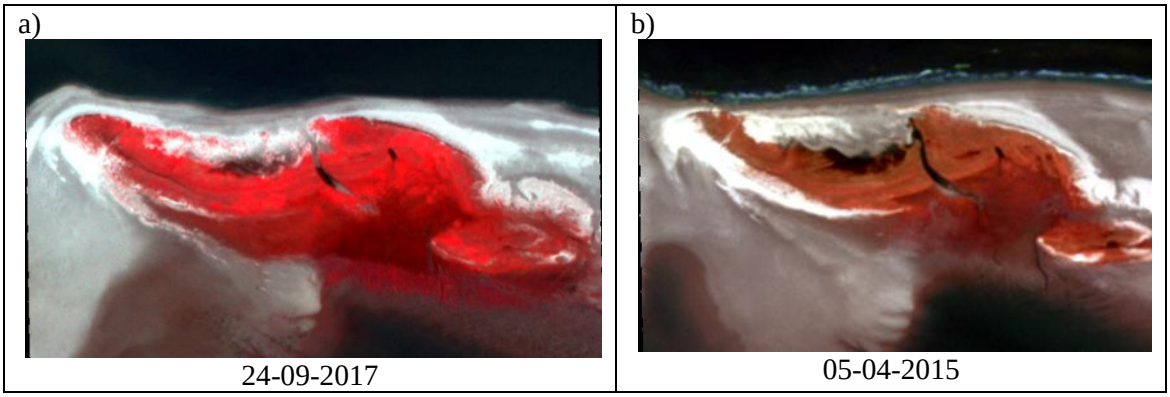

Figure 4.12. False colour (NIR-Red-Green) images showing dark areas (water) in 2017 and similar areas in 2015.

The high water cover at the beginning of 2017 can be explained by the presence of the body of water in the channel, which existed throughout 2017, although its size greatly fluctuated. After mid-February 2018, it greatly shrank in size until it disappears in May 2018. In September, a small body of water reappeared in the same location and was present until at least mid-November, as it is not visible on imagery from 2019 anymore. Visual inspection of RapidEye images revealed the channel has likely had a continuous body of water from the start of image collection in 2009, until it finally disappeared in 2018.

The body of water in the central part of the washover appeared in September 2017 (see Figure 4.12a) and disappeared in February 2018. However, it appeared again in November 2018, disappeared in late February 2019, and briefly appeared again in the next month. The size and the exact location of this second body of water is highly variable. Visual inspection of RapidEye images reveals dark areas in the same region in early 2015 (see Figure 4.12b). These dark areas appear in February and early March, after which they disappear and a vegetated area appears in the same position, only to reappear again in April, and to disappear again in May, after which the boundary between the vegetated and the non-vegetated area appears to have shifted southward.

4.3. Relation between washover development and forcing conditions

Overwash and aeolian transport drive changes from vegetation to sand as vegetation is eroded or buried. Therefore, the area which changed from vegetation to sand between February 2015 and October 2019, compared to the previous image, was investigated. Small changes were usually caused by noise, different light conditions or by small changes in images' spatial position. Therefore, the change maps were manually checked whether the change depicted was a result of noise, or of an actual change in land cover. This was achieved through an analysis of the changed area: if there was a large continuous area changed, it was considered to be an actual change in land cover, while small, irregular changes were considered to be a result of noise. The identified changes are listed in Table 4.1. This list is not exhaustive, there might be more changes which were not observed. Changes from vegetation into sand also happened before 2015, but the low data density makes it difficult to determine if an observed change is the result of one, or of multiple events, and there generally is a large uncertainty regarding the date on which these changes took place, as images are often several months apart. The total water height in Table 4.1 is based on the observed water level at the Huibertgat and the wave set-up, which was assumed to be 20% of the offshore significant wave height (H_s; Masselink et al, 2011). Table 4.1 also shows the area changed and the area permanently changed (the area which did not change back into vegetation later). Because of the different masks, the area permanently changed was not computed for the RapidEye images in 2015 and 2016, as the RapidEye imagery could not be compared with the PlanetScope imagery directly.

The image with the highest water levels is shown in Figure 4.13. There is no overwash in this image, but water levels are considerably higher than in the other images, and the salt marsh in the south of the island is completely inundated. This image was taken an hour before maximum water level. At the time this image was taken, the water level in the Huibertgat was 1.67 metres, and the significant wave height H_s was 3.01 m. This results in a total water level of 2.27 metres during the observed overwash event, which provides insight into which water levels are needed for overwash.

Besides overwash, wind could also have been a factor in turning vegetated areas into sand as a result of aeolian transport. Appendix A shows the wind roses for the periods preceding each change from vegetation to sand as listed in Table 4.1. The wind roses for some of the dates are

missing as a result of missing data. These wind roses are generally quite different from Figure 3.9, as they focus on a more specific period.

Date	Water level [m]	H_s [m]	Total water level [m]	Area [m^2]	Area permanently changed [m^2]
10-03-2015	2.73	5	3.73	15525	-
05-04-2015	2.03	4.64	2.958	6000	-
21-05-2015	1.1	3.67	1.834	18525	-
30-06-2015	1.45	1.53	1.756	3800	-
23-08-2015	1.44	3.46	2.132	14125	-
17-04-2016	2.43	4.3	3.29	21800	-
02-05-2016	1.35	2.34	1.818	5475	-
15-02-2017	2.34	5.53	3.446	55116	8631
27-03-2017	1.76	2.08	2.176	11970	72
29-04-2017	1.38	1.93	1.766	16533	9
15-10-2017	2	4.66	2.932	27603	4113
29-12-2017	2.35	4.81	3.312	23697	954
08-01-2018	2.25	4.18	3.086	9153	567
07-02-2018	1.78	3.61	2.502	13392	2052
19-03-2018	1.23	1.21	1.472	14175	0
04-05-2018	1.47	2.14	1.898	8217	0
03-11-2018	1.8	4.04	2.608	8451	207
03-02-2019	2.56	4.58	3.476	41661	3996
19-03-2019	2.09	1.48	2.386	7623	0
29-10-2019	2.06	-	-	18360	-

Table 4.1. The first column shows the date on which the change from vegetation to sand was observed. The second column shows the maximum water level at the Huibertgat between the image and the previous image, as the overwash must have occurred between the current image and the previous one. The third column shows the significant wave height, H_s. No data was available for 29-10-2019. The fourth column shows the total water level, if the wave set-up is assumed to be 20% of the significant wave height. The fifth column shows the area changed from vegetation to sand compared to the previous image. The area permanently changed denotes the area which changed from vegetation to sand and did not change back to vegetation afterwards.

Figure 4.13. RGB image of Rottumeroog on 08-03-2019, with very high water levels

5. Discussion

The washover displays strong seasonal variation, while the long-term evolution of the washover is characterised by expansion and a southward migration. The seasonal trends will first be analysed, followed by the long-term evolution of the washover. Finally, the washover development will be linked to the forcing conditions.

5.1. Seasonal trends in washover evolution:

The washover generally expands from autumn to early spring, which is in line with the hypotheses, though seasonal variation in storm frequency did not lead to seasonal variation in washover evolution in other studies (Sedrati et al., 2011). The different seasonal pattern in 2015, which shows a small seasonal change with a peak in July, is a result of washover expansion from July to August 2015. The seasonal variation in vegetation cover indicates that vegetation recolonises parts of the washover from late spring to autumn. Reed growing through the deposited sand is unlikely, as this would result in vegetation appearing everywhere in the washover at approximately the same moment in time. This was not the case, as the vegetation appearance follows clear spatial-temporal patterns. Vegetation mostly appeared next to existing vegetation, except for the western part of the washover, where vegetation growth was concentrated on several isolated patches which gradually expanded over time. This is likely due to the local geography: the western part of the washover contains several higher vegetated areas, while the central and eastern parts do not, and generally has a flatter topography (see Figure 2.6). The preferential colonisation of higher areas in the western part of the washover implies that they are easier for vegetation to colonise. Possible explanations include a better-drained subsurface and a reduced salt stress due to less frequent overwash events as a result of the higher elevation.

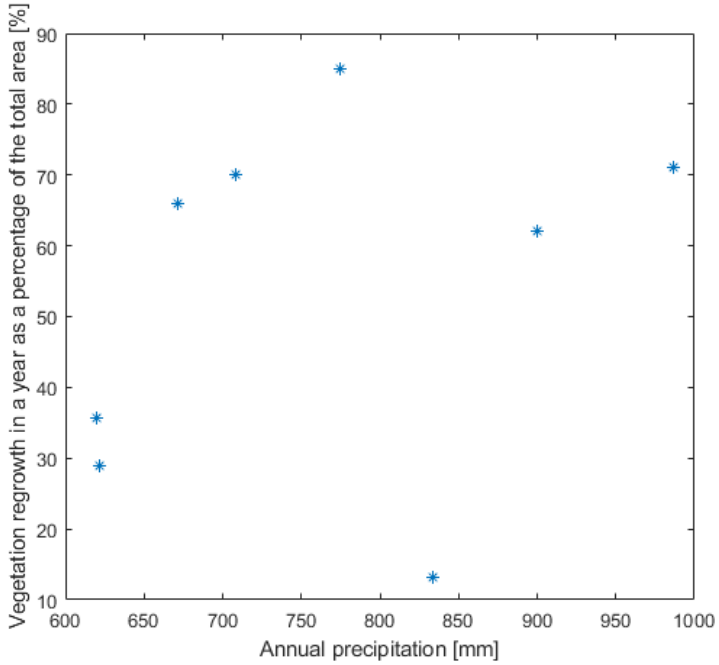

Figure 5.1. The cumulative annual precipitation versus the difference between the maximum and the minimum vegetation in a year as a percentage of the washover area.

It is likely that the amount of vegetation regrowth in a year is significantly influenced by external factors such as the amount of overwash, the temperature and the precipitation. The relatively low amount of vegetation regrowth in 2018 is hypothesised to a result of the relatively low amount of precipitation that year, possibly in combination with the relatively cold winter. However, there is no clear relationship between the amount of precipitation and the percentage of vegetation regrowth in a year (as measured by the difference between the minimum and the maximum vegetated area for a year), as can be seen in Figure 5.1. The years before 2012 were excluded because the amount of seasonal regrowth exceeded 100% due to definition issues.

The amount of seasonal regrowth (as measured by the difference between the minimum and the maximum vegetation cover) as a percentage of the washover area is typically at 70% (± 10%). It is hypothesised that conditions were relatively favourable for vegetation growth from 2012 to 2013 as the washover was partially sheltered by dunes in the east, which would reduce the amount of overwash events. When these dunes eroded in 2014, conditions in the washover became less favourable to vegetation growth and the percentage of regrowth decreased. It is hypothesised that the continued supply of sediment to the washover elevated a large part of the washover enough to make conditions more favourable for vegetation from 2015 to 2016, allowing for more vegetation growth. From 2016 to 2019, the location of the seasonal vegetation growth has shifted from being just outside the washover, towards washover itself, as evidenced by the decrease in vegetation cover in the northeast and an increase in the washover itself (see Figure 4.6). This is interpreted to be a result of the continuing coastal erosion on the seaward side of the island, and the continued increase in elevation in the washover, which continues to make the washover more favourable for vegetation growth.

The seasonal recolonisation of vegetation was not attested in other studies on washovers (e.g. Nielsen & Nielsen, 2006; Mathew et al., 2010; Aagaard & Kroon, 2019). Whether this is a result of different conditions, or of the coarse temporal timescale of other studies is not known and should be investigated in future research. Nielsen & Nielsen (2006) presumed that the repeated overwash resulted in an environment that is too saline for vegetation to colonise. This study shows that vegetation can already colonise a washover months after a washover event. As the washover on Rottumeroog shows no signs of a recovery of the dune system, the development of vegetation on the washover might be less significant in causing new foredune growth than previously thought (Aagaard & Kroon, 2019). It is hypothesised that foredune growth will only be possible at a later stage where the washover is elevated to such an extent that overwash will be extremely uncommon.

The non-permanent body of water which appeared in the central part of the washover is hypothesised to form because of several factors. Firstly, this area is relatively low compared to its surroundings. Secondly, it is inferred that the subsurface consists of an impermeable clay layer, as this area used to be a salt marsh before the washover formed. It is hypothesised that the appearance of this body of water is related to the amount of precipitation. The first appearance of this body of water on the PlanetScope imagery was in September 2017, a month with an extremely large amount of precipitation (168.8 mm). As no large areas changed from vegetation

into sand, it is concluded that no washovers took place. The appearance of the body of water is therefore likely a result of the extreme precipitation. In contrast, this body of water also appears in November 2018, when the precipitation is only 21.9 mm. It is therefore considered that the body of water must have appeared as a result of an overwash event in late October or early November 2018. The dark areas in 2015 are considered to be a similar body of water, and are likely also the result of overwash, as the precipitation in these months is relatively low. The short reappearance of the body of water in March 2019 can either have been a result of high precipitation or of overwash.

5.2. Long-term trends in washover evolution:

The unvegetated areas from 2009 to 2010 are not considered to be part of the washover, as the boundary between the vegetated and the unvegetated area is in a very different spatial position before 2012 (see Figure 4.7). Therefore, the washover is considered to have formed between the 1st of October 2011, and the 25th of May 2012. This is supported by the lack of washover expansion from 2009 to 2011, in contrast to later years (except for 2012-2013), when the washover is characterised by a strong expansion. Furthermore, in Figure 4.4, the difference between the minimum and maximum vegetation cover is larger than the washover area itself for 2010 and 2011. This is likely because of changes just outside the washover, but it implies as a lack of significant seasonal variation in the washover itself, which is different from the years afterwards, when the washover does experience seasonal variation. The formation of the washover in 2011 or 2012 is in line with the hypothesis that the washover formed between 2007 and 2013, but closer to 2013 than to 2007. The unvegetated areas from 2009 to 2011 might still have aided in the development of the washover, as these areas were relatively low compared to the surrounding dunes (see Figure 2.6a and b).

A possible explanation for the lack of washover expansion from 2012 to (April) 2013 is that dunes to the east of the washover were blocking its expansion (see Figure 2.6c). These dunes disappear in 2014, as the area where they used to be is no longer vegetated. It is therefore suggested that a storm strong enough to erode the dunes did not occur from 2012 to 2013. The storm which eroded the dunes must have occurred between the 28th of September 2013 and the 30th of May 2014. This is hypothesised to be a result of the storm surge of 5 December 2013 (Spencer et al., 2015). The eastward expansion of the washover from 2014 onwards continued until the washover reached the dunes on the south side of the island. This implies that the washover has difficulty expanding beyond higher parts of the island such as dune rows, likely because the wave energy has already been dissipated before the waves reach the dunes. The lack of a westward expansion of the washover can also be explained by the presence of dunes and higher areas in the west of the island (see Figure 2.6d). The expansion of the washover to the southeast, into the channel, is also explained by the absence of dunes in this area. Overall, the washover shows an expanding trend and there are no signs of a permanent recovery of the dune system. The decrease in washover area in 2019 is considered to be a result of a shift from vegetation regrowth just outside the washover to vegetation regrowth inside the washover, which

results in a reduction of the washover area. The expanding trend of the washover is in line with the hypotheses, and is consistent with other studies, which also did not find a permanent recovery of the dune system in washovers in the first few years after the washover was first formed (Mathew et al., 2010; Aagaard & Kroon, 2019).

The expansion of the washover was coupled with a strong onshore retreat of the island of 150-200 metres, as evidenced by the retreat of the boundary between the unvegetated and the vegetated area directly west of the washover. This is in line with the findings of Wesselman (2019). The onshore migration of the island is likely a result of overwash, as the beach did not have a clear eroding trend before the washover formed, and the island only started migrating southwards after the formation of the washover in 2012. The likely explanation for the erosion of the beach is that sand from the beach is deposited in the washover during overwash and as a result of aeolian transport.

It is hypothesised that although the water table has been lowered in the former channel (or possibly, the elevation has been raised as sediment was deposited), it is still too wet for vegetation to colonise. The temporary reappearance of the lake in late 2018 also indicates that the channel is likely still relatively wet compared to the surrounding areas. It is unlikely that the washover is kept open by aeolian transport, as there are likely no 3D effects, which would accelerate aeolian transport in the channel because of the limited variation in elevation, and because there is no indication of sediment being deposited on the landward side of the channel.

Rottumeroog does not fit well into either of the stable states of barrier islands proposed by Durán Vinent & Moore (2014), as the island is affected by both vegetation recovery and overwash. There is no sign of a recovery of the dune system (which would lead to a typical ‘high’ island as described by Durán Vinent & Moore (2014)), but the island is also not trapped in a perpetual state of low elevation, as the island is gaining in height. It is therefore suggested that there might be a third stable state, where both overwash and vegetation growth affect the island, with neither being dominant enough to lead to the formation of a typical ‘high’ or ‘low’ island. It is however possible that there is a hysteresis in island response (Durán Vinent & Moore, 2014). Further research should indicate whether a third stable state exists, and under which circumstances it would apply, as the conditions at barrier islands in the Wadden Sea are markedly different from those at barrier islands at the Atlantic coast of the United States, where hurricanes have a major impact on washover development (Williams, 2015).

5.3. Relation between washover development and forcing conditions

It is likely that all major changes from vegetation to sand on Rottumeroog are either a result of overwash or of aeolian transport. Based on Figure 4.13, it is estimated that a total water level of at least 2-2.5 metres is needed for overwash. Overwash with a total water level below metres is probably not possible. This implies that the observed change events with their highest total water level below 2 metres were all caused by aeolian activity. The wind roses were also compared to the location of the areas changed from vegetation into sand relative to the washover. Out of the 20 observed changes, 10 had a total water level above 2.5 metres in the period between

the previous image and the image on which the change was observed. Therefore, these 10 changes were caused by overwash.

6 changes had a total water level below 2 metres in the period between the previous image and the image on which the change was observed and were therefore not caused by overwash. For five of these images, the prevailing wind direction in the preceding period indicates that aeolian transport would be in the direction of the changed area. The change in these images is therefore concluded to be a result of aeolian activity. For one image, the prevailing wind direction did not match the area where the changes were observed. It is hypothesised that the change was caused by aeolian transport by northerly winds, which were uncommon in this period.

The remaining four images had a total water level between two and 2.5 metres. For two of these images, the prevailing wind direction did not match the area where the changes were observed, and in another image, the sand was wet. These three changes were therefore concluded to be a result of overwash. The fourth image (taken on 23-08-2015) had vegetation growth in the western part of the washover, while the washover expanded in the eastern part. The continued vegetation growth implies that no washovers took place. However, there was no clear prevailing wind direction in this period. It is possible that the westerly and northerly winds in this period transported sand to the southwest, despite the most common wind direction being from the east. Another explanation would be that overwash took place, which only affected the eastern part of the washover, allowing the vegetation in the higher western part of the washover to continue to grow.

A summary of the different causes for change is provided in Table 5.1.

Date on which the change was observed	Total water level [m]	Area [m^2]	Area permanently changed [m^2]	Cause of change
10-03-2015	3.73	15525	-	Overwash
05-04-2015	2.958	6000	-	Overwash
21-05-2015	1.834	18525	-	Aeolian
30-06-2015	1.756	3800	-	Aeolian
23-08-2015	2.132	14125	-	Unresolved
17-04-2016	3.29	21800	-	Overwash
02-05-2016	1.818	5475	-	Aeolian
15-02-2017	3.446	55116	8631	Overwash
27-03-2017	2.176	11970	72	Overwash
29-04-2017	1.766	16533	9	Aeolian
15-10-2017	2.932	27603	4113	Overwash
29-12-2017	3.312	23697	954	Overwash
08-01-2018	3.086	9153	567	Overwash
07-02-2018	2.502	13392	2052	Overwash
19-03-2018	1.472	14175	0	Aeolian
04-05-2018	1.898	8217	0	Aeolian (hypothesised)
03-11-2018	2.608	8451	207	Overwash
03-02-2019	3.476	41661	3996	Overwash
19-03-2019	2.386	7623	0	Overwash
29-10-2019	2.06+	18360	-	Overwash

Table 5.1. Cause of observed changes. The total water level is the water level, assuming the wave set-up is 20% of H_s. The area denotes the area changed from vegetation to sand. The area permanently changed denotes the area which changed from vegetation to sand and did not change back to vegetation afterwards.

Both overwash and aeolian processes affected the washover. Figure 5.2 shows the distribution of the observed changes shown in Table 5.1 throughout the year, revealing a seasonal pattern. Washovers occur exclusively from October to April (with the possible exception of the unresolved event in August). The number of overwash events (based on Table 5.1) is high in October, as would be expected from the high average maximum water level in that month (see Figure 3.5). However, the number of washovers is relatively low in the months afterwards (until February), even though the average maximum water level in these months is much higher than in spring, when washovers are more common. This is hypothesised to be a result of the low data density from November to January: as there are few images available, there are likely more overwash events than the amount of observed changes. The observed seasonal variation in washover frequency is in line with the hypothesis that seasonal patterns in overwash lead to seasonal patterns in morphological development, which contrasts with Sedrati et al (2011).

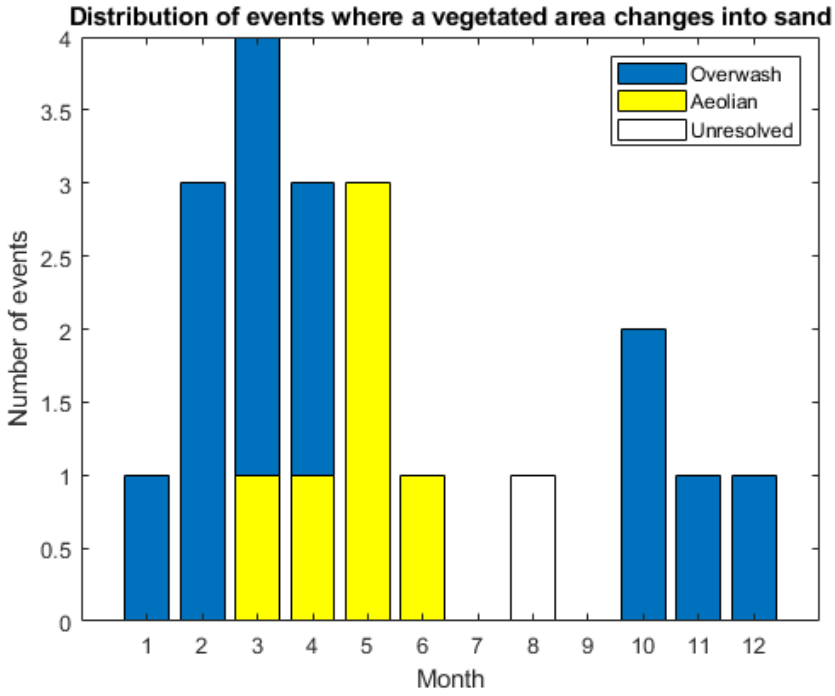

Figure 5.2. Distribution of events where a vegetated area changed into sand, based on the date on which they were observed. Note that the bars are stacked.

The aeolian changes all occurred between March and May, suggesting a strong seasonal pattern in aeolian transport. It was originally hypothesised that aeolian transport would occur in the summer months, but the vegetation growth in summer and autumn likely prevents aeolian transport as the fetch is reduced. Reduced aeolian transport in the summer months was also observed on other Wadden Sea islands, such as in blowouts on Schiermonnikoog (Maas, 2020). The continued overwash from late autumn to early spring results in sand which is too wet for aeolian transport. This only leaves the spring months for significant aeolian transport.

Table 5.1 shows that aeolian transport lead to almost no permanent changes in land cover. This implies that overwash is more important for the long-term evolution of the washover, as the aeolian changes all seasonal. The area which changed permanently scales with the total area changed as a result of overwash, as can be seen in Figure 5.3. It is hypothesised that it is more difficult for vegetation to recolonise a larger area than a smaller area, leading to a larger area which is not recolonised by vegetation.

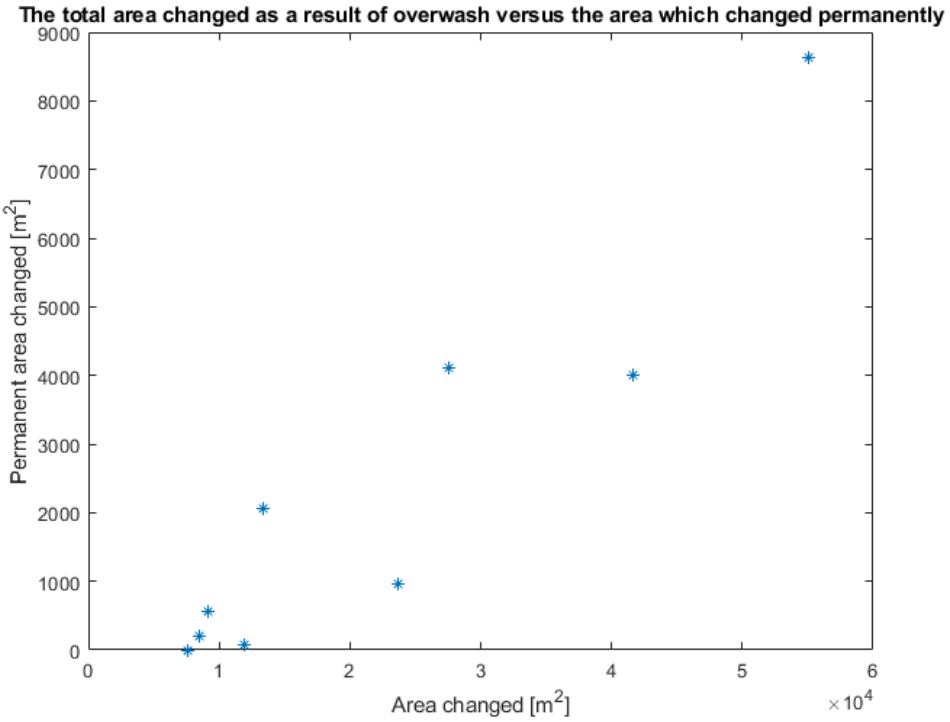

Figure 5.4. The area changed as a result of overwash versus the area which permanently changed from vegetation to sand.

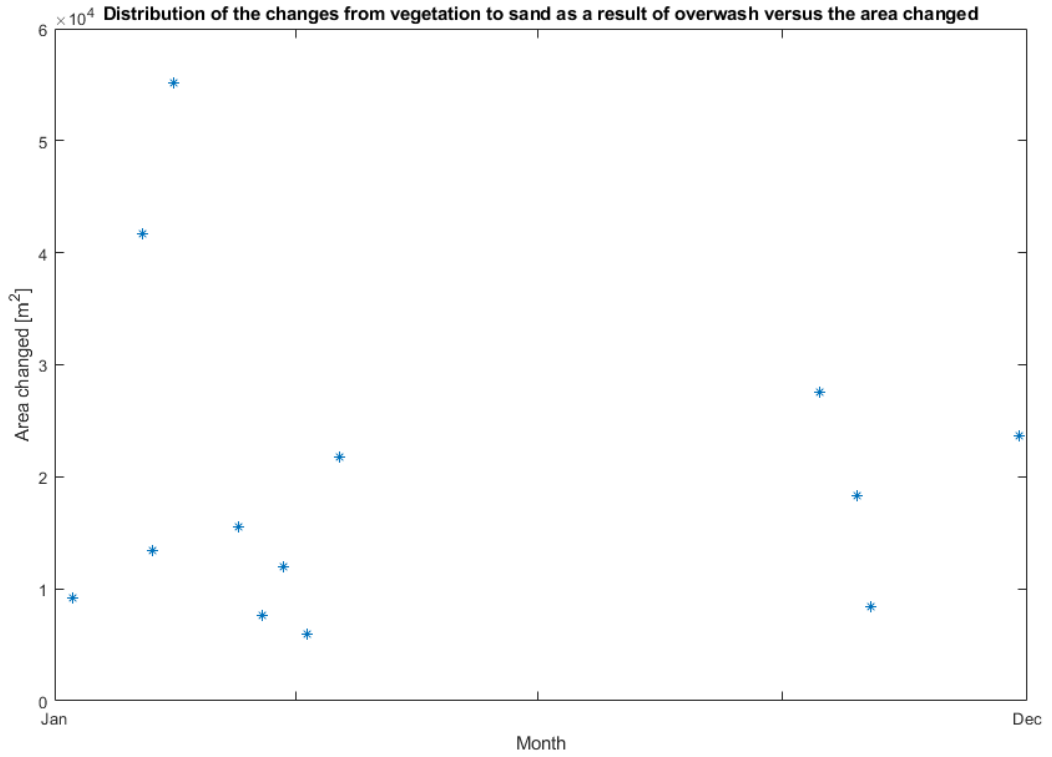

Figure 5.4. The area changed as a result of overwash for different overwash events, sorted by time of the year.

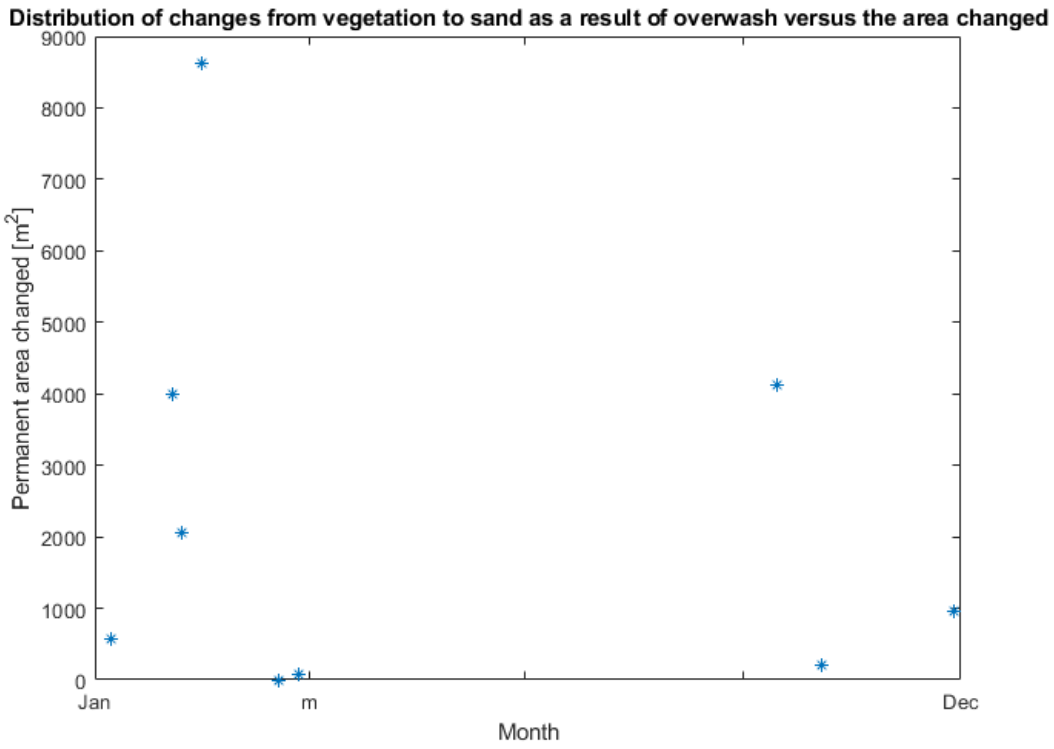

Figure 5.5. The area which permanently changed as a result of overwash for different overwash events, sorted by time of the year.

Figure 5.4 shows the distribution of the area eroded for each overwash event (as listed in Table 5.1). There is no clear pattern between the area changed and the month when the changes occur. The two largest changed both occur early in the year. This is likely a result of the low data density in these months: as the were no images in the preceding period, multiple overwash events were likely only visible in the same image and were therefore counted as one overwash event with a very large area changed. Figure 5.5 shows the same distribution, but then for the area which permanently changed from vegetation to sand. There is also no clear pattern between the area which permanently changed and the time of the year, though this might be related to lack of data.

The relationship between the total water level and the area which changed from vegetation to sand as a result of the overwash is shown in Figure 5.6. This relationship is not significant. The area changed from vegetation to sand likely depends on many other factors besides the water level, such as the overwash duration, the topography, and the pre-overwash presence of vegetation. It is also possible that other variables, such as the sand volume deposited, would give a better indication of the magnitude of overwash events. The exact factors which determine the changed area (or volume) are suggested as topics for future research. There also appears to be no relationship between the area changed from vegetation to sand and the cause for the change, though the largest changes (>20000 m^2 changed) were all caused by overwash.

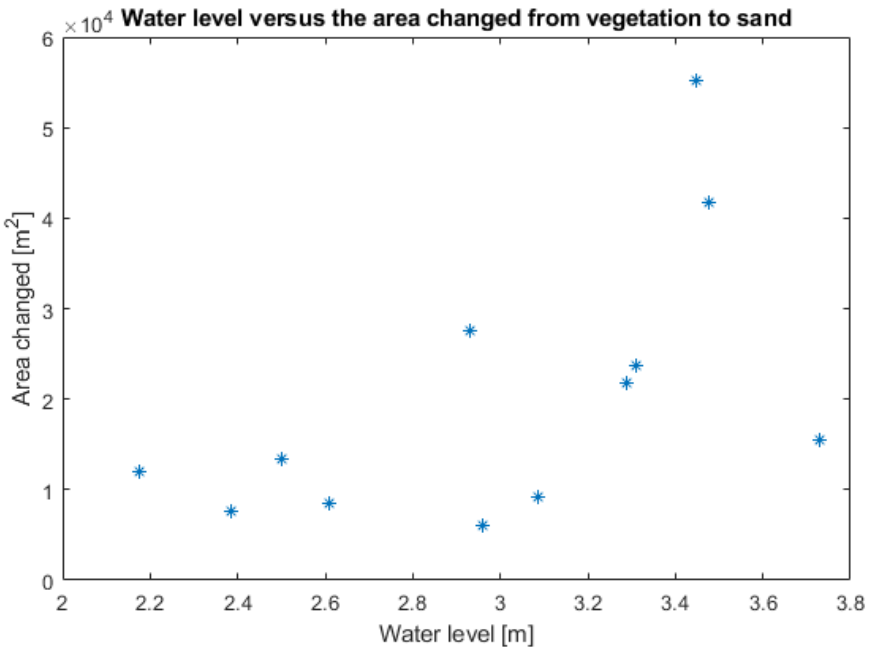

Figure 5.6. The maximum water level in the period before the image was taken versus the area which changed from vegetated to sand.

6. Conclusion

Re-activation of washovers, after they were closed off by sand drift dikes, is currently being considered in the Netherlands (Wesselman et al., 2017; Wesselman, 2019). This would allow barrier islands to grow with sea-level rise in a natural way. However, washover evolution after washover formation has received little attention in the past (Aagaard & Kroon, 2019). This study has therefore investigated the washover on Rottumeroog on various timescales, and provided new insight on washover evolution, especially concerning the seasonal scale, as the seasonal patterns observed here have not been observed at other washovers. The seasonal patterns provide insight into the occurrence of overwash events and their effect on washover evolution.

The washover formed between the 1st of October 2011, and the 25th of May 2012. The washover remained stable throughout 2012 and 2013. It is hypothesised that dunes on the eastern side of the washover were blocking its expansion and sheltering the washover from overwash. These dunes were eroded from 2013 to 2014, after which the washover rapidly expanded towards the south and the east. This expansion continued until the washover reached the dunes on the southern side of the island, which implies that higher areas such as dunes form a natural border for washovers, beyond which expansion is difficult. The washover expanded from $6.1 \cdot 10^4$ m^2 in 2012 to $9.3 \cdot 10^4$ m^2 in 2019, peaking in 2018 at $1.3 \cdot 10^5$ m^2. The expansion of the washover was coupled with a migration of the island of 150-200 metres in the landward direction, which is considered to be a direct result of the presence of a washover, as overwash erodes sediment from the beach and deposits it in the washover. The observed patterns of washover expansion are consistent with previous literature and observations on Rottumeroog (Wesselman, 2019).

The washover displays clear seasonal variation as vegetation cover is high in autumn and low in spring, which is a result of a seasonal variation in washover frequency and vegetation regrowth. The observed overwash events all occurred from October to April, with the highest washover frequency in October and from February to April. The unexpectedly low amount of washovers from November to January is likely a result of the low data density in these months. The area which changed from vegetation to sand as a result of the overwash did not scale with the water level in the preceding period. The frequent overwash in winter causes the vegetation in the washover to disappear and inhibits aeolian transport as the sand is too wet. As washover frequency decreases in spring, aeolian transport picks up. All changes caused by aeolian transport occurred from March to June. Vegetation growth also starts in spring as conditions become more favourable, showing that vegetation growth is already possible shortly after a washover. This contrasts with Nielsen & Nielsen (2006), who suggested that the repeated overwash would make the washover too saline for vegetation to colonise. Vegetation growth is concentrated in patches on the western side of the washover, while in the middle and eastern parts of the washover, vegetation growth is adjacent to the existing vegetation. The continued vegetation growth eventually reduces the fetch by the start of summer, reducing aeolian transport. The vegetation peaked between September and November. Aeolian transport did not lead to any permanent land cover changes, which suggests that overwash is more important in determining the long-term evolution of the washover.

The amount of vegetation regrowth is typically 70% of the washover area (±10%). At first, the washover was sheltered by dunes to the northeast, which reduce overwash and create relatively favourable conditions for vegetation growth. As these dunes were eroded in 2014, conditions in the washover became less favourable for vegetation and the amount of regrowth dropped. In 2016, the amount of vegetation regrowth suddenly increased. This is likely a result of the continued sediment transport to the washover, which elevated the washover enough to make conditions more favourable for vegetation growth. Low vegetation regrowth rates in 2018 are hypothesised to have been caused by low precipitation. From 2016 to 2019, the location of vegetation regrowth has shifted being just outside the washover towards the washover itself, as the elevation inside the washover increased and coastal erosion made the seaward areas less favourable for vegetation. The increase in vegetation in the washover is also hypothesised to have caused the disappearance of the lake in the former channel.

The current state of Rottumeroog suggests that there might be more than two stable states for barrier islands, as Rottumeroog does not fit well into the existing classification by Durán Vinent & Moore (2014), which distinguishes high islands dominated by aeolian activity and vegetation recovery from low islands which are dominated by washovers. Rottumeroog might represent an intermediate case where both processes are important, though overwash appears to be more important for the long-term evolution of the washover.

References:

Aagaard, T., & Kroon, A., 2019. Decadal behaviour of a washover fan, Skallingen Denmark. *Earth Surface Processes and Landforms* 44, 1755-1768.

Durán Vinent, O., Moore, L.J., 2014. Barrier island bistability induced by biophysical interactions. Nature climate change 5, 158-162.

Engelstad, A., 2019. Hydrodynamics and cross-shore sand transport during barrier island inundation (Thesis).

Hoekstra, P., Haaf, M. T., Buijs, P., Oost, A., Breteler, R. K., van der Giessen, K., & van der Vegt, M. (2009). Washover development on mixed-energy, mesotidal barrier island systems. *Coastal Dynamics* 83, 25 32.

Hesp, P.A., Hyde, R., 1996. Flow dynamics and geomorphology of a trough blowout. *Sedimentology* 43, 505–525.

Hosier, P. E., & Cleary, W. J., 1977. Cyclic geomorphic patterns of washover on a barrier island in southeastern North Carolina. *Environmental Geology* 2, 23-31.

Löffler, M. A. M., Grootjans, A. P., c. C. de Leeuw, Oost, A. P., & Verbeek, S. K. (2008). Eilanden natuurlijk: natuurlijke ontwikkeling en veerkrcht op de Waddeneilanden. 1st edition, Groningen, the Netherlands: *Het Grafisch Huis*.

Lorenzo-Trueba, J., Ashton, A.D., 2013. Rollover, drowning, and discontinuous retreat: Distinct modes of barrier response to sea-level rise arising from a simple morphodynamic model. *Journal of Geophysical Research: Earth Surface* 119, 779-801.

Maas, B.F., 2020. Mapping the recent bio-geomorphological evolution of the man-made Terschelling blowout complex using PlanetScope imagery and airborne LiDAR data. (Master Thesis)

Masselink, G., Hughes, M.G., Knight, J., 2011. Introduction to coastal processes and geomorphology. 2nd edition, New York, USA: *Routledge*.

Mathew, S., Davidson-Arnott, R. G., & Ollerhead, J., 2010. Evolution of a beach–dune system following a catastrophic storm overwash event: Greenwich Dunes, Prince Edward Island, 1936–2005. *Canadian Journal of Earth Sciences* 47, 273-290.

Nielsen, N., & Nielsen, J., 2006. Development of a washover fan on a transgressive barrier, Skallingen, Denmark. *Journal of Coastal Research* 39, 107-111.

Oost, A. P., Hoekstra, P., Wiersma, A., Flemming, B., Lammerts, E. J., Pejrup, M., Hofstede, J., van der Valk, B., Kiden, P., Bartholdy, J., van der Berg, M. W., Vos, P.C., de Vries, S., Wang, Z.B., 2012. Barrier island management: Lessons from the past and directions for the future. *Ocean & Coastal Management* 68, 18-38.

Pereira, D., 2015. WindRose for Matlab. Retrieved from: https://www.scribd.com/document/313556032/WindRose-Doc.

Planet Labs, 2019. Planet imagery product specifications. Retrieved from: https://assets.planet.com/docs/Planet_Combined_Imagery_Product_Specs_letter_screen.pdf

Roy, S., 2019. samapriya/porder: porder: Simple CLI for Planet ordersV2 API (Version 0.5.5). Zenodo. http://doi.org/10.5281/zenodo.3533213

Sedrati, M., Ciavola, P., & Armaroli, C., 2011. Morphodynamic evolution of a microtidal barrier, the role of overwash: Bevano, Northern Adriatic Sea. *Journal of Coastal Research* 64, 696-700.

Schemmekes, L.M., 2020. Long-term morphodynamic development of blowouts in Zuid-Kennemerland determined with PlanetScope imagery and airborne LiDAR data. (Master thesis)

Spencer, T., Brooks, S.M., Evans, B.R., Tempest, J.A., Möller, I. Southern North Sea stormsurge event of 5 December 2013: Water levels, waves and coastal impacts. *Earth-Science Reviews* 146, 120-145.

Wesselman, D., van der Vegt, M., & de Winter, R., 2017. The influence of washover dimensions and beach characteristics on the sediment transport during inundation. *Coastal Dynamics 2017*, Paper No. 265.

Wesselman, D., 2019. The morphological response to storms at Rottumeroog; an island without active coastal management since 2005 (Chapter of a thesis, work in progress).

Wesselman, D., de Winter, R., Oost, A., Hoekstra, P., & van der Vegt, M., 2019. The effect of washover geometry on sediment transport during inundation events. *Geomorphology* 327, 28-47.

Williams, H.F.L., 2015. Contrasting styles of Hurricane Irene washover sedimentation on three east coast barrier islands: Cape Lookout, North Carolina; Assateague Island, Virginia; and Fire Island, New York. *Geomorphology* 231, 182-192.

Appendix A. Wind roses

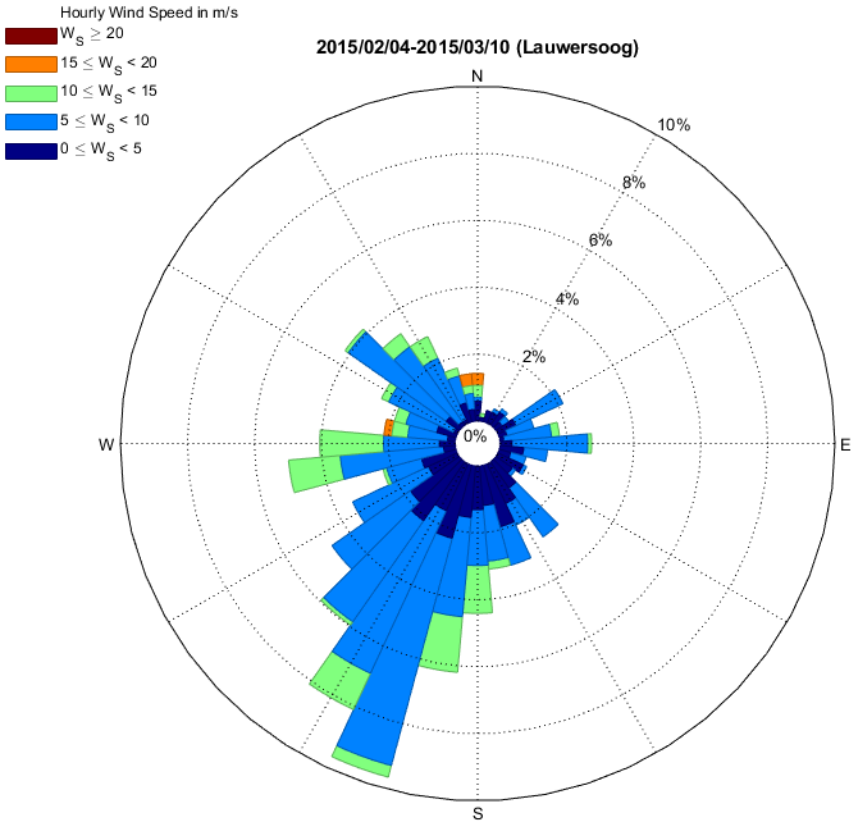

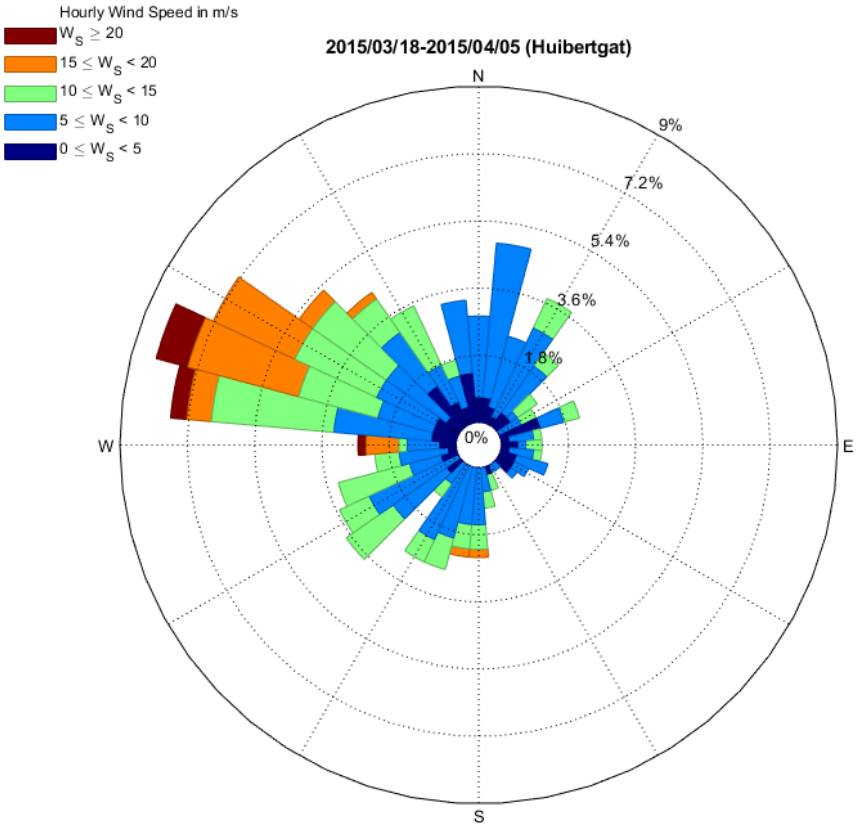

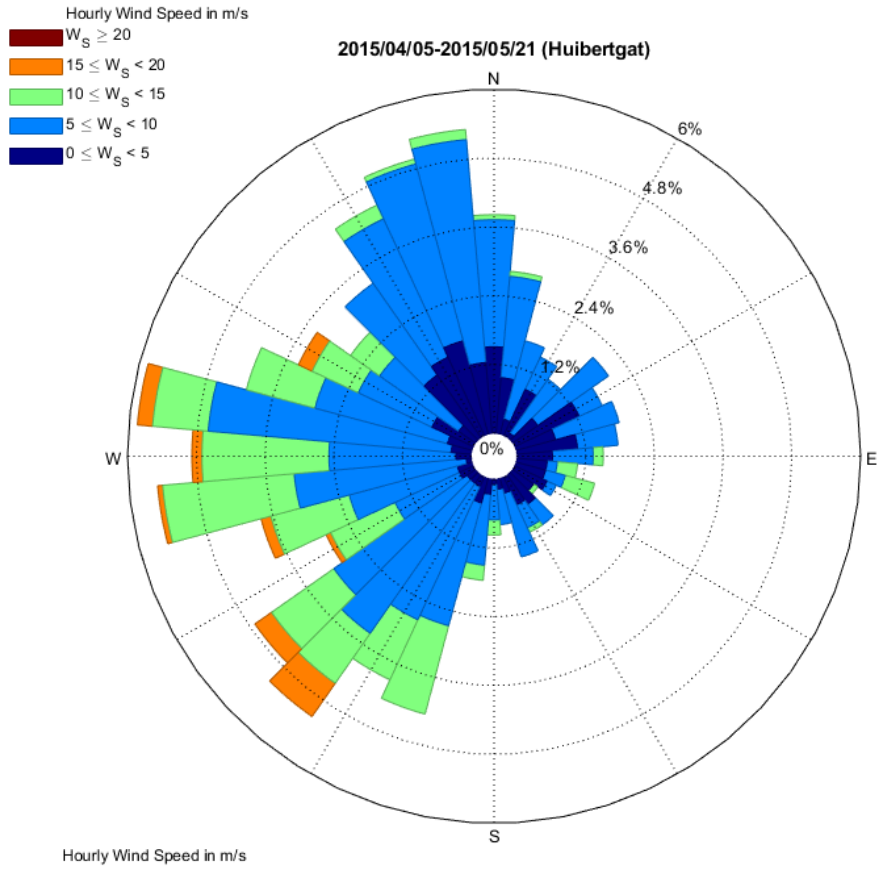
Hourly Wind Speed in m/s
$W_S \geq 20$
$15 \leq W_S < 20$
$10 \leq W_S < 15$
$5 \leq W_S < 10$
$0 \leq W_S < 5$
2015/04/05-2015/05/21 (Huibertgat)
N
E
S
W
6%
4.8%
3.6%
2.4%
1.2%
0%

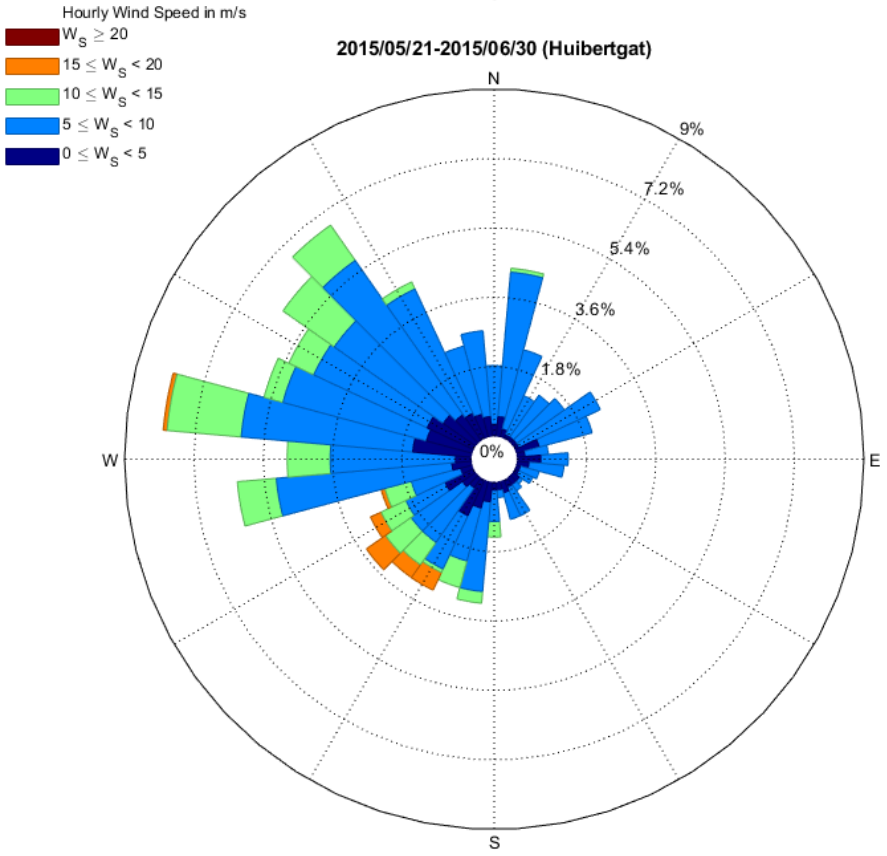
Hourly Wind Speed in m/s
$W_S \geq 20$
$15 \leq W_S < 20$
$10 \leq W_S < 15$
$5 \leq W_S < 10$
$0 \leq W_S < 5$
2015/05/21-2015/06/30 (Huibertgat)
N
E
S
W
9%
7.2%
5.4%
3.6%
1.8%
0%

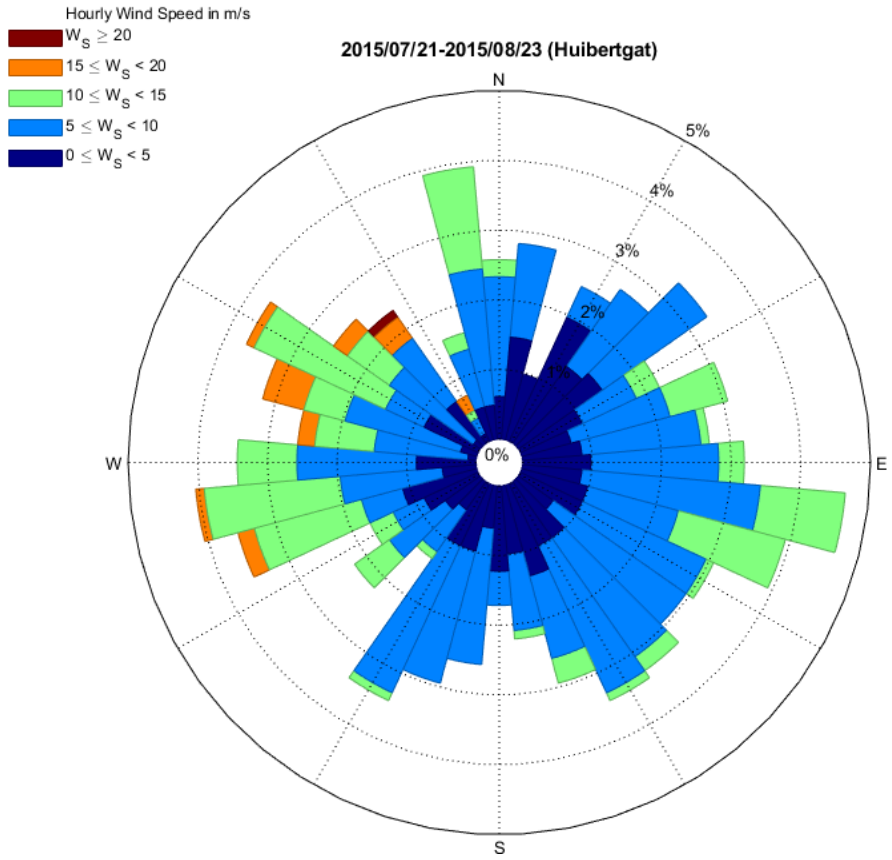
Hourly Wind Speed in m/s
W_S ≥ 20
15 ≤ W_S < 20
10 ≤ W_S < 15
5 ≤ W_S < 10
0 ≤ W_S < 5
2015/07/21-2015/08/23 (Huibertgat)
N
5%
4%
3%
2%
1%
0%
W
E
S

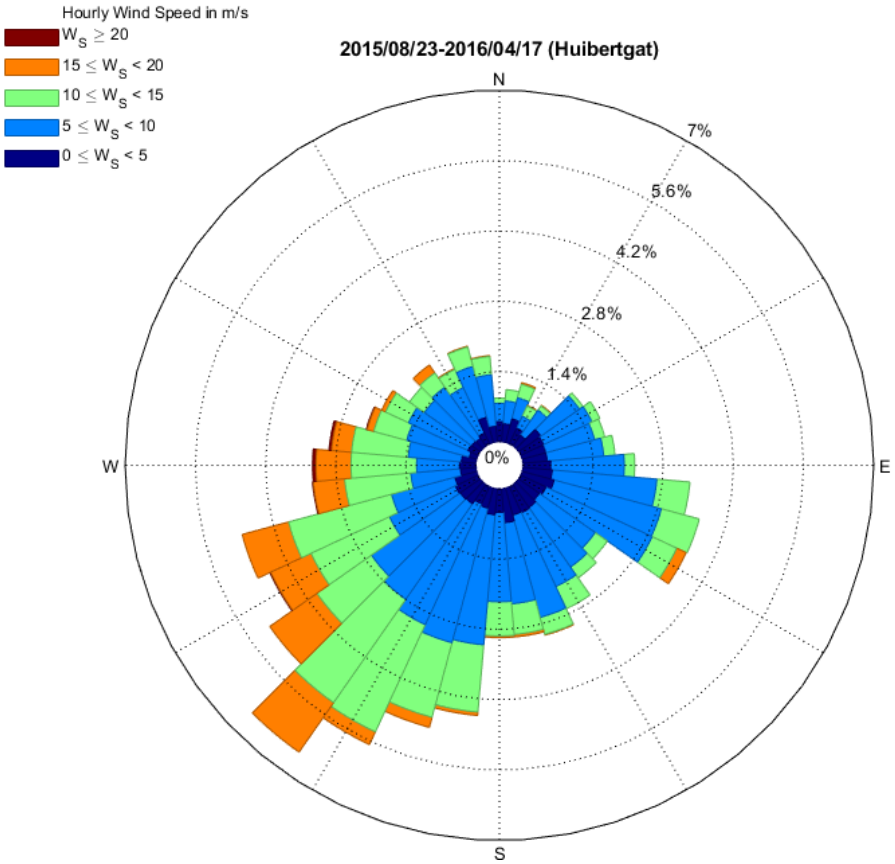
Hourly Wind Speed in m/s
W_S ≥ 20
15 ≤ W_S < 20
10 ≤ W_S < 15
5 ≤ W_S < 10
0 ≤ W_S < 5
2015/08/23-2016/04/17 (Huibertgat)
N
7%
5.6%
4.2%
2.8%
1.4%
0%
W
E
S

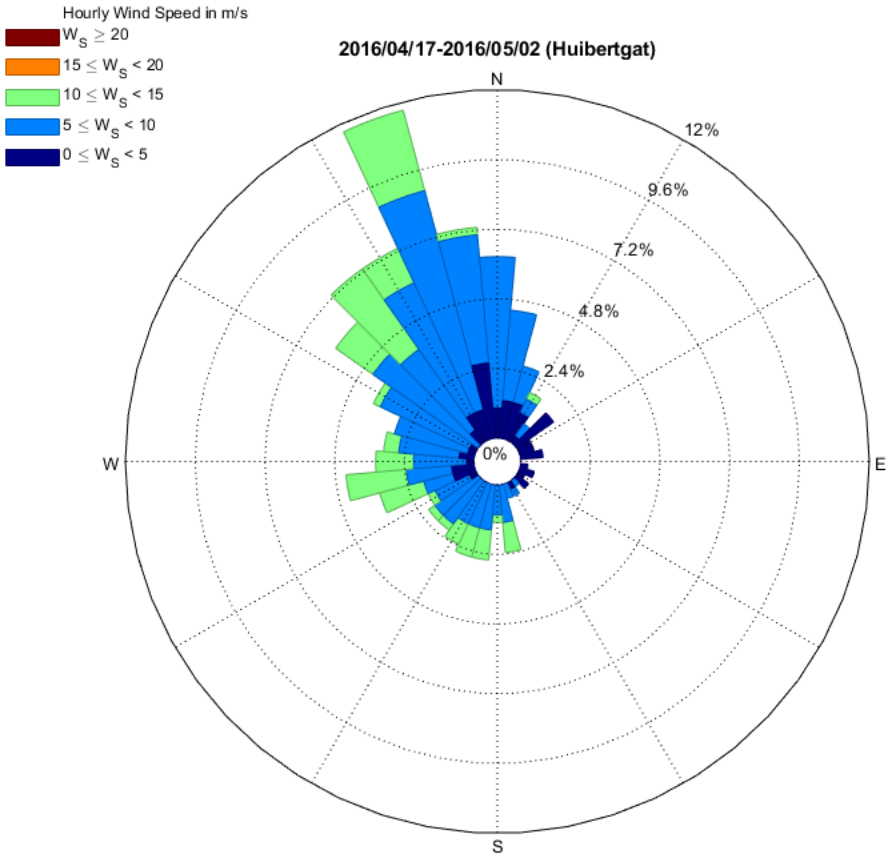
Hourly Wind Speed in m/s
W_S ≥ 20
15 ≤ W_S < 20
10 ≤ W_S < 15
5 ≤ W_S < 10
0 ≤ W_S < 5
2016/04/17-2016/05/02 (Huibertgat)
N
12%
9.6%
7.2%
4.8%
2.4%
0%
W
E
S

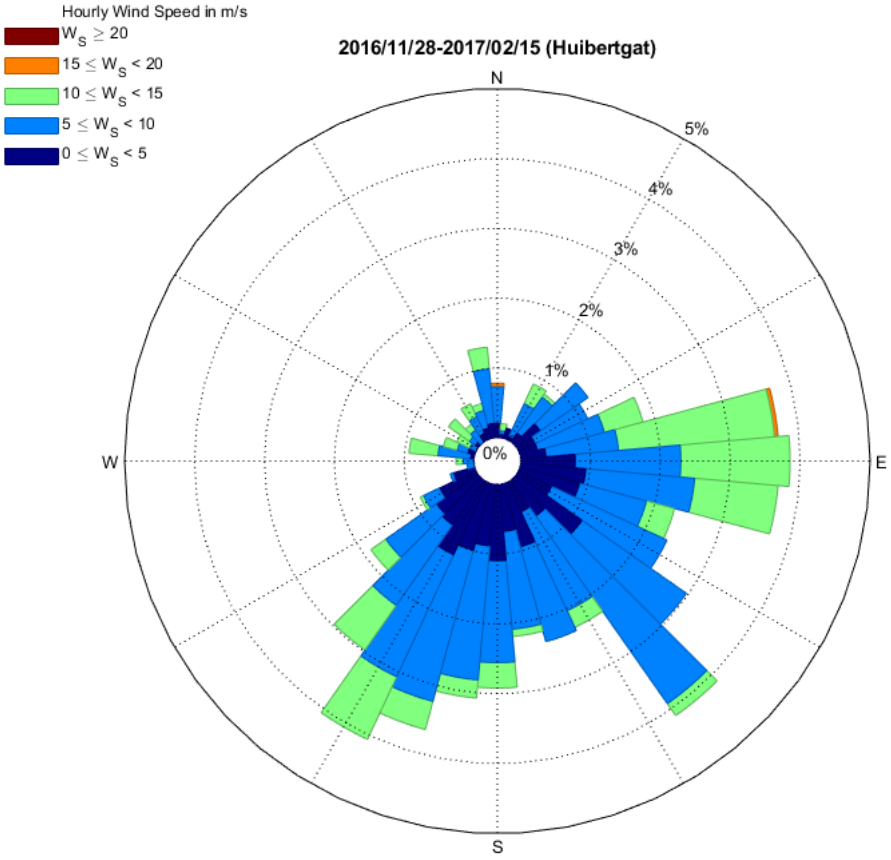
Hourly Wind Speed in m/s
W_S ≥ 20
15 ≤ W_S < 20
10 ≤ W_S < 15
5 ≤ W_S < 10
0 ≤ W_S < 5
2016/11/28-2017/02/15 (Huibertgat)
N
5%
4%
3%
2%
1%
0%
W
E
S

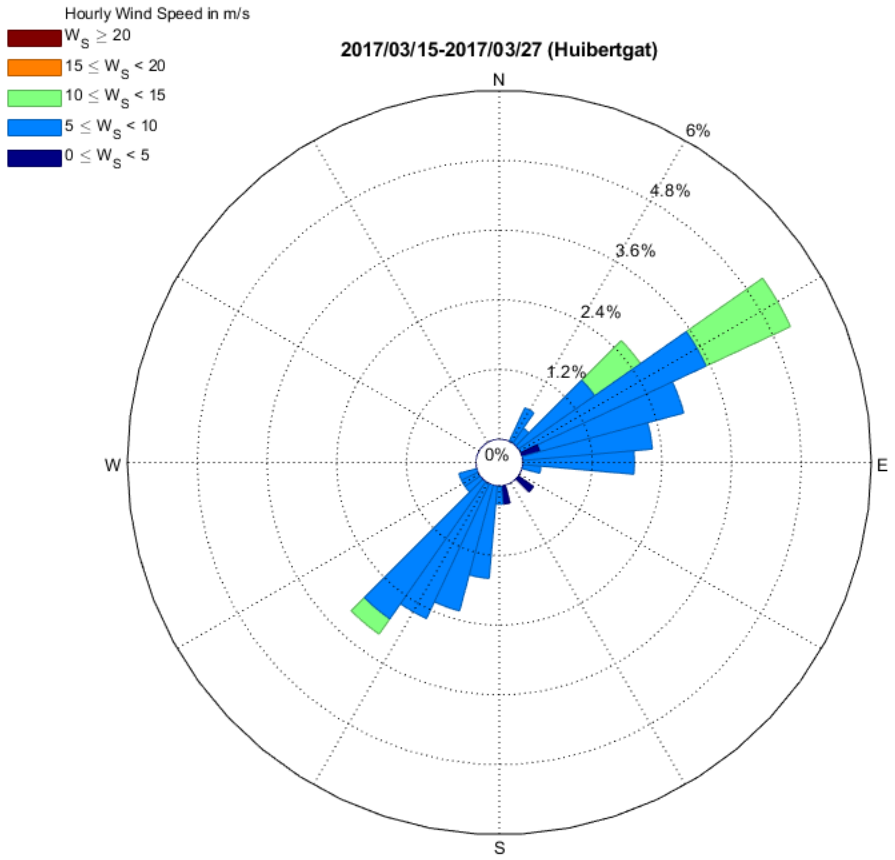
Hourly Wind Speed in m/s
W_S ≥ 20
15 ≤ W_S < 20
10 ≤ W_S < 15
5 ≤ W_S < 10
0 ≤ W_S < 5
2017/03/15-2017/03/27 (Huibertgat)
N
E
S
W
6%
4.8%
3.6%
2.4%
1.2%
0%

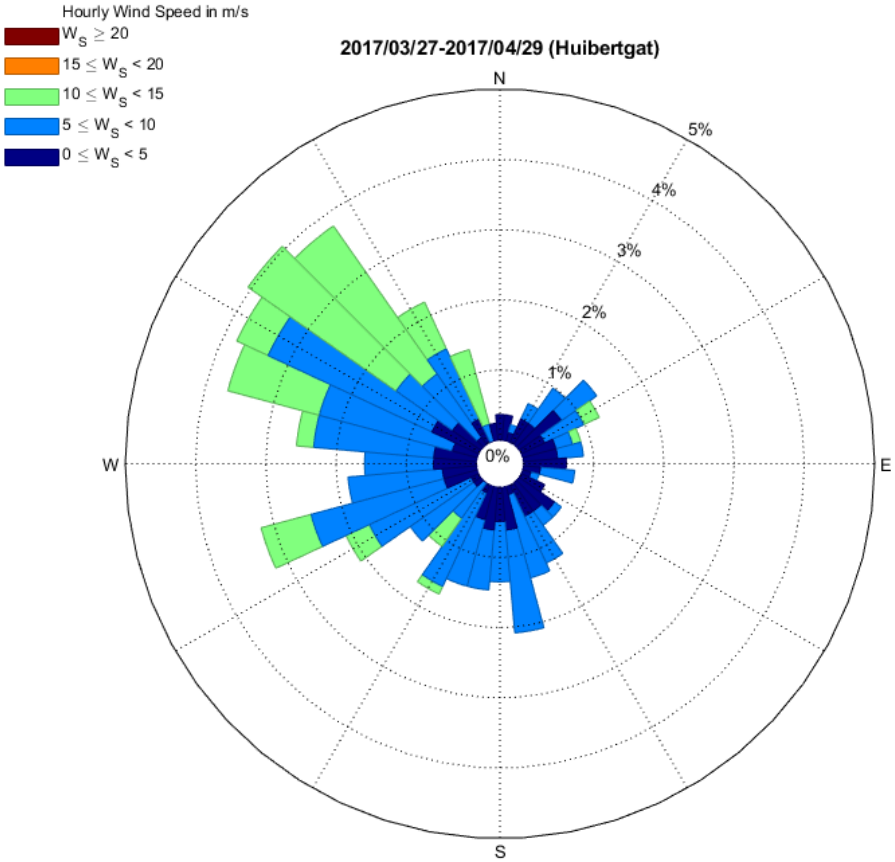
Hourly Wind Speed in m/s
W_S ≥ 20
15 ≤ W_S < 20
10 ≤ W_S < 15
5 ≤ W_S < 10
0 ≤ W_S < 5
2017/03/27-2017/04/29 (Huibertgat)
N
E
S
W
5%
4%
3%
2%
1%
0%

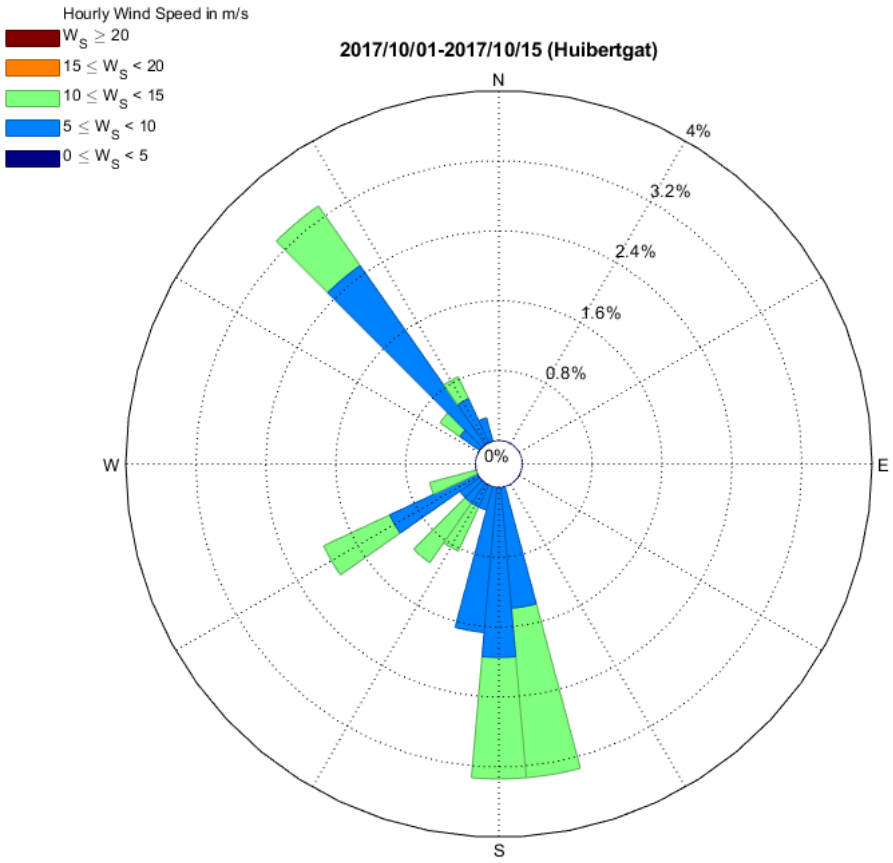
Hourly Wind Speed in m/s
W_S ≥ 20
15 ≤ W_S < 20
10 ≤ W_S < 15
5 ≤ W_S < 10
0 ≤ W_S < 5
2017/10/01-2017/10/15 (Huibertgat)
N
E
S
W
4%
3.2%
2.4%
1.6%
0.8%
0%

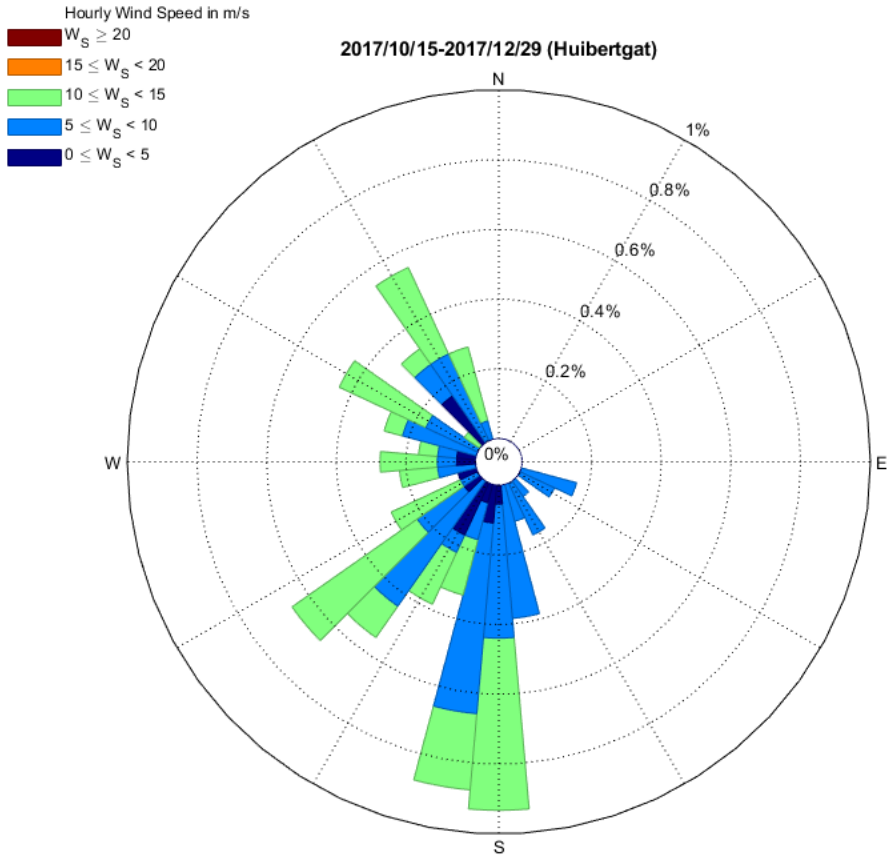
Hourly Wind Speed in m/s
W_S ≥ 20
15 ≤ W_S < 20
10 ≤ W_S < 15
5 ≤ W_S < 10
0 ≤ W_S < 5
2017/10/15-2017/12/29 (Huibertgat)
N
E
S
W
1%
0.8%
0.6%
0.4%
0.2%
0%

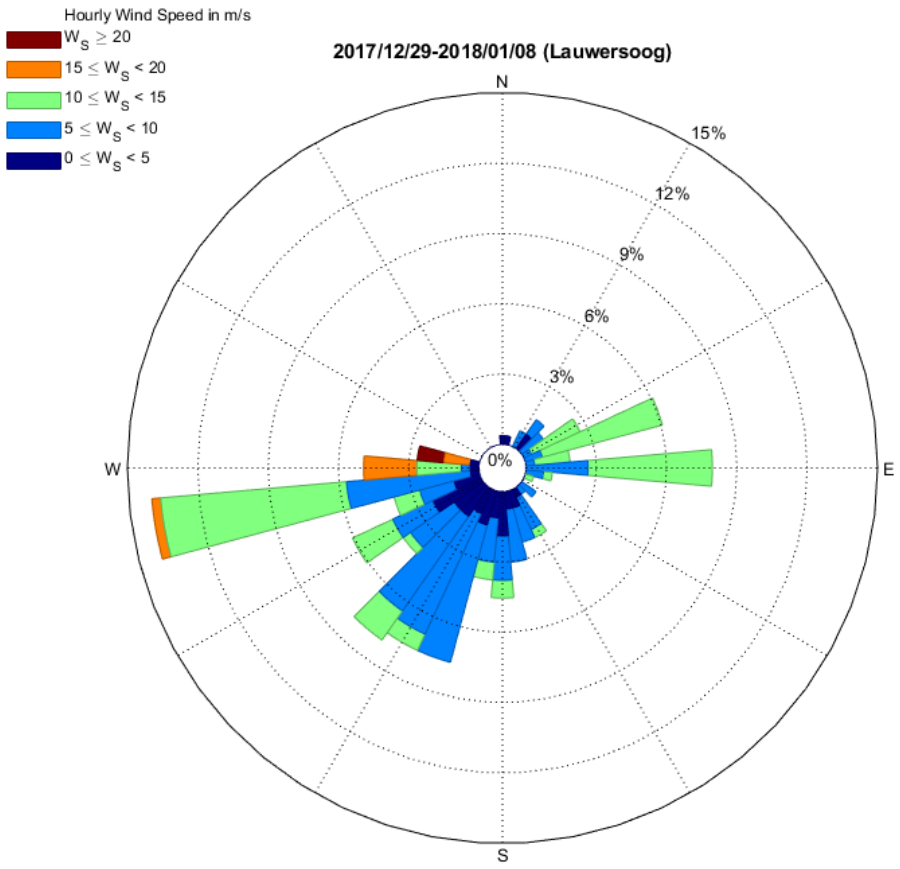
Hourly Wind Speed in m/s
W_S ≥ 20
15 ≤ W_S < 20
10 ≤ W_S < 15
5 ≤ W_S < 10
0 ≤ W_S < 5
2017/12/29-2018/01/08 (Lauwersoog)
N
E
S
W
15%
12%
9%
6%
3%
0%

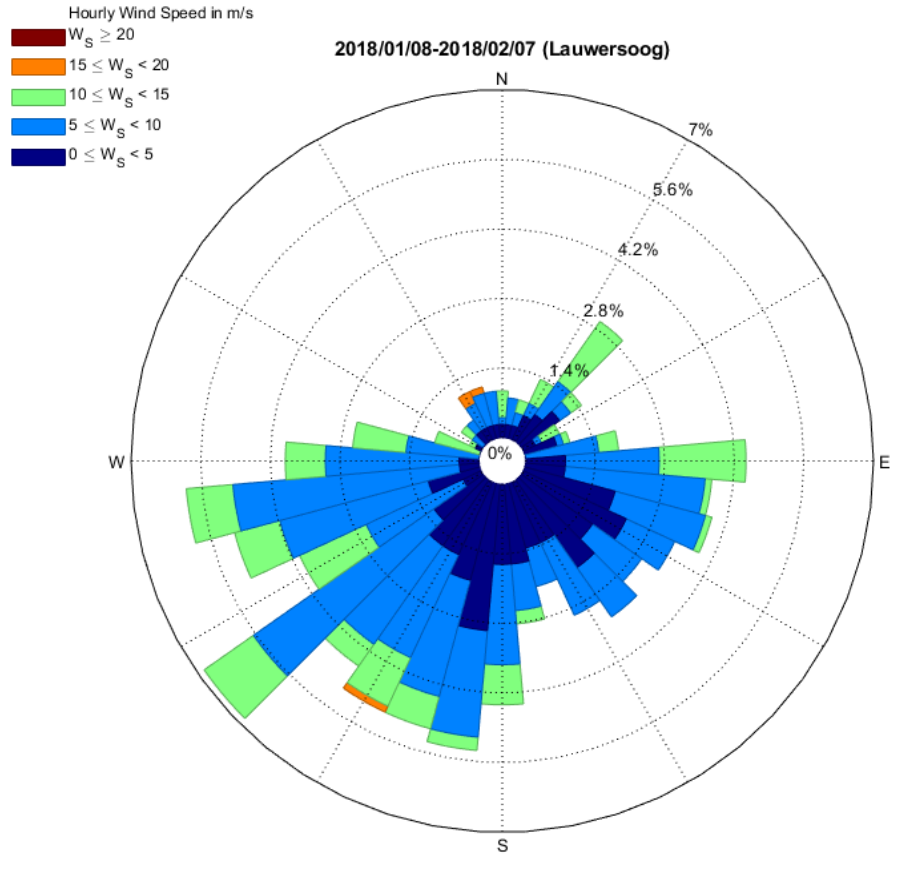
Hourly Wind Speed in m/s
W_S ≥ 20
15 ≤ W_S < 20
10 ≤ W_S < 15
5 ≤ W_S < 10
0 ≤ W_S < 5
2018/01/08-2018/02/07 (Lauwersoog)
N
E
S
W
7%
5.6%
4.2%
2.8%
1.4%
0%

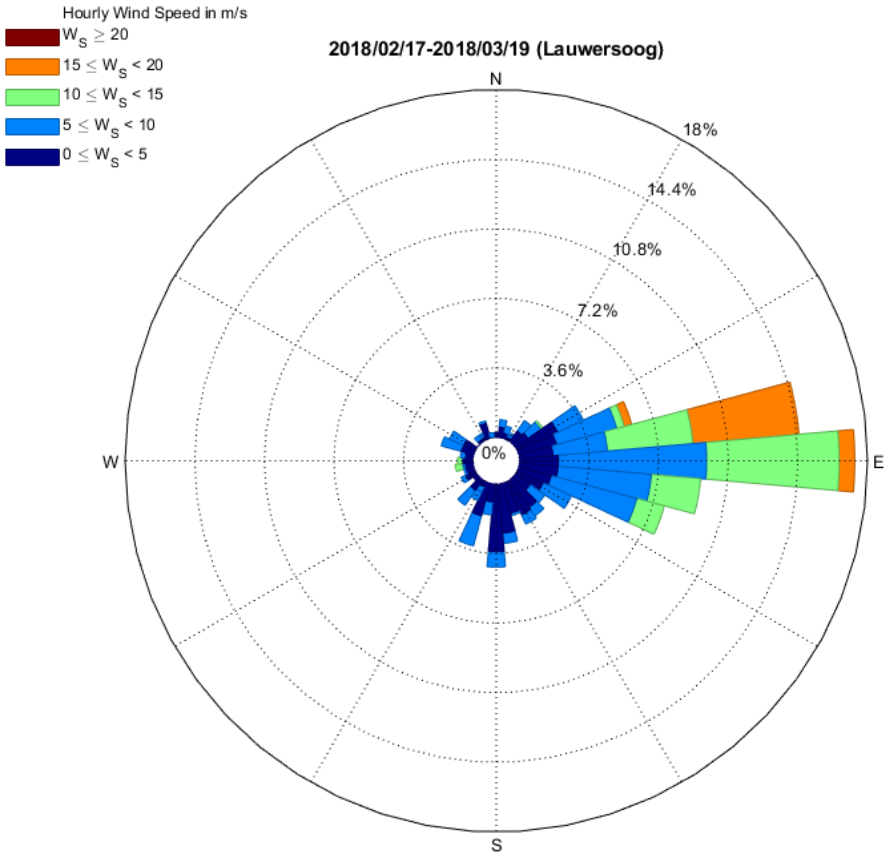
Hourly Wind Speed in m/s
W_S ≥ 20
15 ≤ W_S < 20
10 ≤ W_S < 15
5 ≤ W_S < 10
0 ≤ W_S < 5
2018/02/17-2018/03/19 (Lauwersoog)
N
18%
14.4%
10.8%
7.2%
3.6%
0%
W
E
S

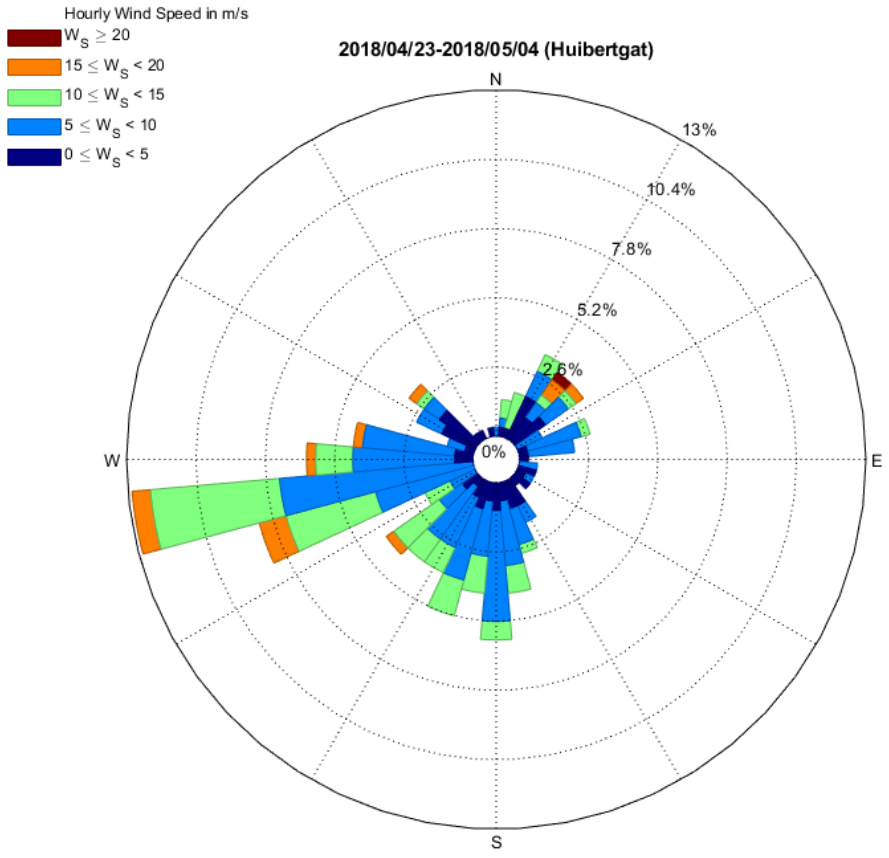
Hourly Wind Speed in m/s
W_S ≥ 20
15 ≤ W_S < 20
10 ≤ W_S < 15
5 ≤ W_S < 10
0 ≤ W_S < 5
2018/04/23-2018/05/04 (Huibertgat)
N
13%
10.4%
7.8%
5.2%
2.6%
0%
W
E
S

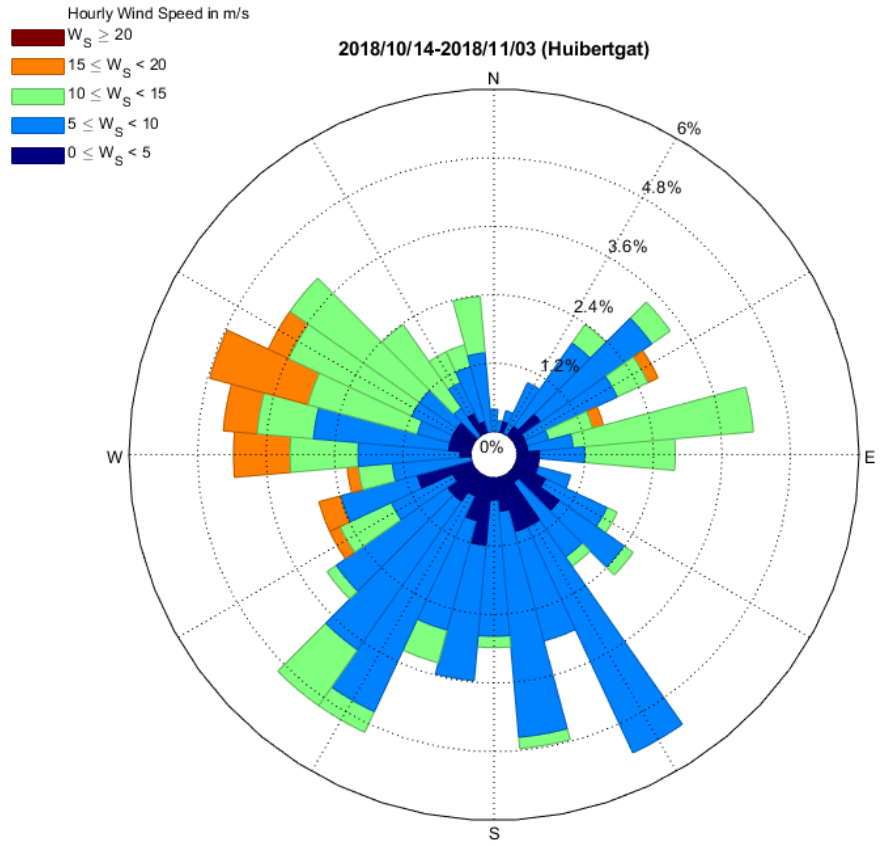
Hourly Wind Speed in m/s
W_S ≥ 20
15 ≤ W_S < 20
10 ≤ W_S < 15
5 ≤ W_S < 10
0 ≤ W_S < 5
2018/10/14-2018/11/03 (Huibertgat)
N
6%
4.8%
3.6%
2.4%
1.2%
0%
W
E
S

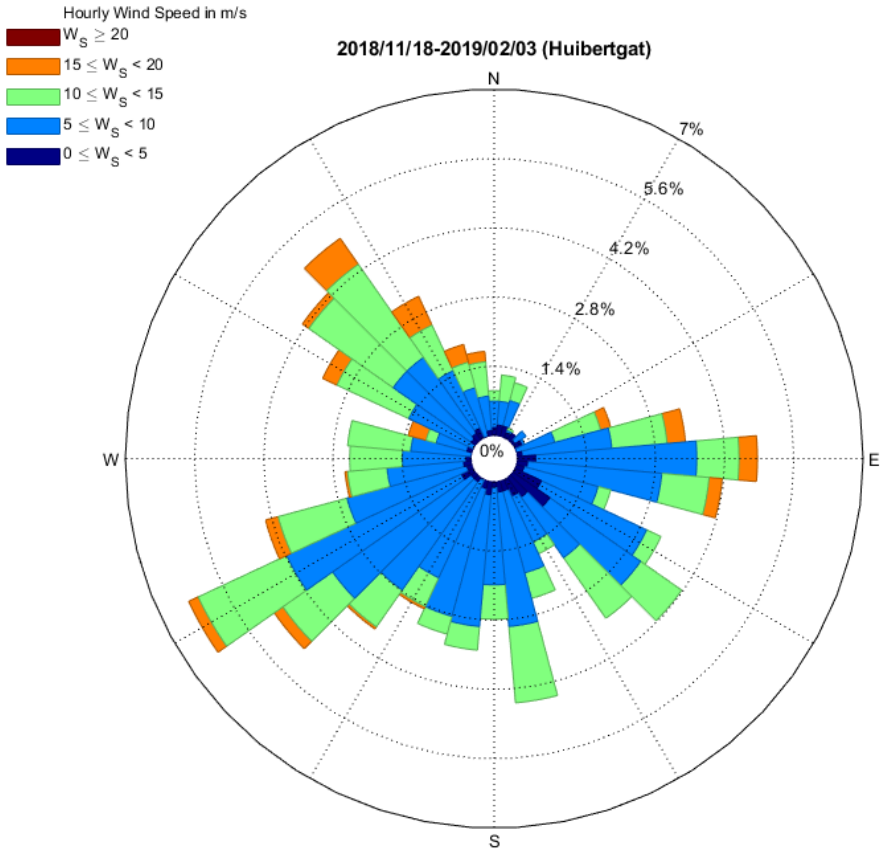
Hourly Wind Speed in m/s
W_S ≥ 20
15 ≤ W_S < 20
10 ≤ W_S < 15
5 ≤ W_S < 10
0 ≤ W_S < 5
2018/11/18-2019/02/03 (Huibertgat)
N
7%
5.6%
4.2%
2.8%
1.4%
0%
W
E
S

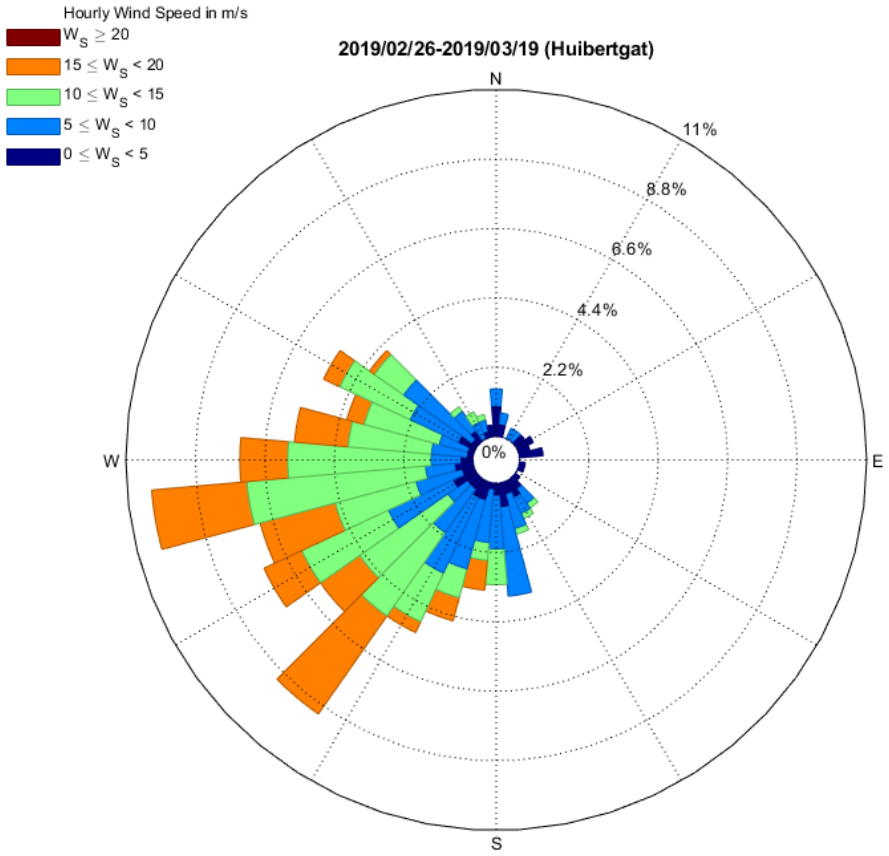
Hourly Wind Speed in m/s
W_S ≥ 20
15 ≤ W_S < 20
10 ≤ W_S < 15
5 ≤ W_S < 10
0 ≤ W_S < 5
2019/02/26-2019/03/19 (Huibertgat)
N
11%
8.8%
6.6%
4.4%
2.2%
0%
W
E
S

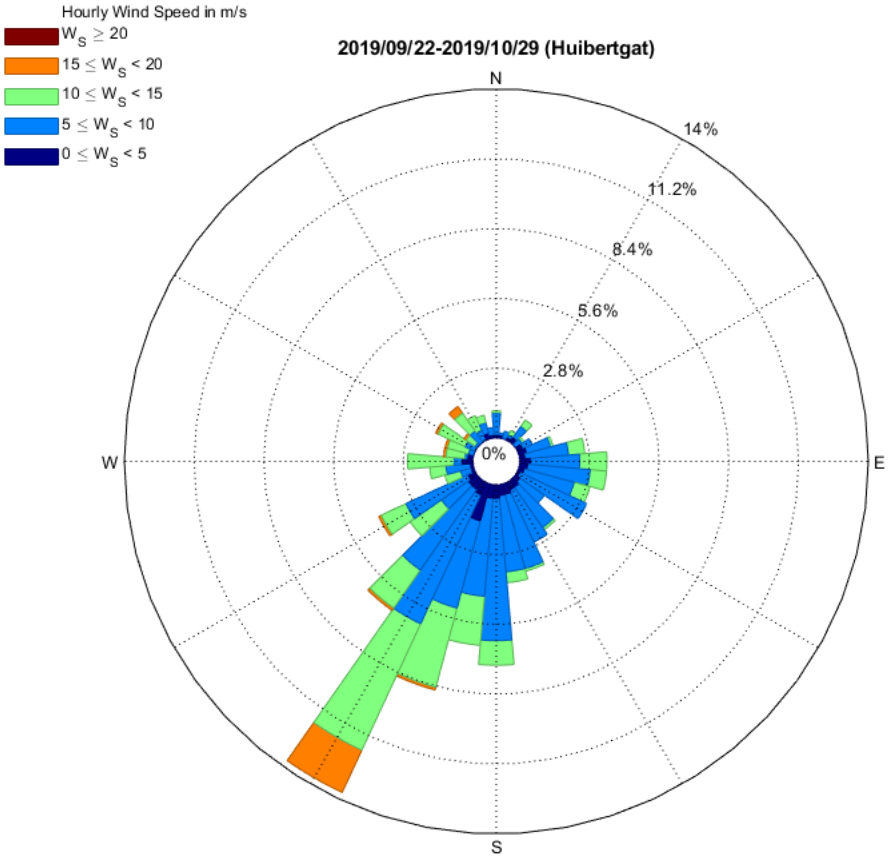
Hourly Wind Speed in m/s
W_S ≥ 20
15 ≤ W_S < 20
10 ≤ W_S < 15
5 ≤ W_S < 10
0 ≤ W_S < 5
2019/09/22-2019/10/29 (Huibertgat)
N
14%
11.2%
8.4%
5.6%
2.8%
0%
W
E
S